The evolution and star formation of dwarf galaxies in the Fornax Cluster

M. J. Drinkwater,[1]★ M. D. Gregg,[2,3] B. A. Holman[1] and M. J. I. Brown[1,4]

[1]*School of Physics, University of Melbourne, Victoria 3010, Australia*
[2]*Department of Physics, University of California at Davis, Davis, CA 95616, USA*
[3]*Institute for Geophysics and Planetary Physics, Lawrence Livermore National Laboratory, L-413, Livermore, CA 94550, USA*
[4]*National Optical Astronomy Observatory, 950 North Cherry Avenue, PO Box 26732, Tucson, AZ 85726, USA*

ABSTRACT

We present the results of a spectroscopic survey of 675 bright ($16.5 < b_J < 18$) galaxies in a $6°$ field centred on the Fornax cluster with the FLAIR-II spectrograph on the UK Schmidt Telescope. Three galaxy samples were observed: compact galaxies to search for new blue compact dwarfs, candidate M 32-like compact dwarf ellipticals, and a subset of the brightest known cluster members in order to study the cluster dynamics. We measured redshifts for 516 galaxies, of which 108 were members of the Fornax Cluster. Defining dwarf galaxies to be those with $b_J \geq 15$ ($M_B \geq -16.5$), there are a total of 62 dwarf cluster galaxies in our sample. Nine of these are new cluster members previously misidentified as background galaxies. The cluster dynamics show that the dwarf galaxies are still falling into the cluster whereas the giants are virialized.

We classified the observed galaxies as late-type if we detected Hα emission at an equivalent width greater than 1 Å. The spectra were obtained through fixed apertures, so they reflect activity in the galaxy cores, but this does not significantly bias the classifications of the compact dwarfs in our sample. The new classifications reveal a higher rate of star formation among the dwarf galaxies than suggested by morphological classification: 35 per cent have significant Hα emission indicative of star formations but only 19 per cent were morphologically classified as late-types.

The star-forming dwarf galaxies span the full range of physical sizes and we find no evidence in our data for a distinct class of star-forming blue compact dwarf (BCD) galaxy. The distribution of scale sizes is consistent with evolutionary processes which transform late-type dwarfs to early-type dwarfs. The fraction of dwarfs with active star formation drops rapidly towards the cluster centre: this is the usual density–morphology relation confirmed here for dwarf galaxies. The star-forming dwarfs are concentrated in the outer regions of the cluster, the most extreme in an infalling subcluster. We estimate gas depletion time-scales for five dwarfs with detected H I emission: these are long (of order 10^{10} yr), indicating that an active gas removal process must be involved if they are transformed into gas-poor dwarfs as they fall further into the cluster. Finally, in agreement with our previous results, we find no compact dwarf elliptical (M 32-like) galaxies in the Fornax Cluster.

Key words: stars: formation – galaxies: dwarf – galaxies: evolution – galaxies: clusters: individual: Fornax.

1 INTRODUCTION

Our understanding of the role of dwarf galaxies in clusters has long been dominated by photographic studies of the nearest clusters. The major surveys of the Virgo cluster in the north (Binggeli, Sandage & Tarenghi 1984; Binggeli, Sandage & Tammann 1985; Binggeli, Popescu & Tammann 1993) and the Fornax cluster in the

south (Ferguson & Sandage 1988; Ferguson 1989b) have established the presence of large populations of dwarf galaxies in these clusters. Lacking redshift information, these works have had to rely on image morphology for statistical separation of cluster members from the large contamination of background objects.

When the Fornax Cluster Catalogue (FCC; Ferguson 1989b) was compiled, only 85 of the 340 likely cluster members had measured redshifts; of the whole FCC of 2678 galaxies, only 112 (4 per cent) had redshifts. Since then, a number of small-scale spectroscopic

★E-mail: m.drinkwater@physics.unimelb.edu.au

surveys have been made of the cluster (Held & Mould 1994; Bureau, Mould & Staveley-Smith 1996; Hilker et al. 1999), but even as recently as 1999, NED[1] still lists only about 120 objects within a 5° radius of NGC 1399 with velocities that would place them in the cluster. In this paper we describe a large new spectroscopic investigation of the Fornax cluster designed to add radial velocity membership, spectral classification and dynamical information to the existing knowledge of the cluster. Our study is based on data from the FLAIR-II spectrograph on the UK Schmidt Telescope. We measured the redshifts of over 500 galaxies brighter than $b_J = 18$ in the direction of Fornax, of which 108 are members of the cluster. This study is complementary to the Fornax Cluster Spectroscopic Survey (FCSS), Drinkwater et al. (2000b), which uses the Two degree Field (2dF) spectrograph on the Anglo-Australian Telescope to make a deeper survey of a smaller region towards the centre of the cluster. Unlike the current study, the FCSS will measure *all* objects in its target magnitude range ($16.5 < b_J < 19.7$), irrespective of morphology (i.e. both 'stars' and 'galaxies') in order to sample the largest possible range of surface brightness.

A number of issues regarding the Fornax dwarf population can be addressed definitively only through spectroscopic information in order to determine cluster membership. One interesting question is the possible existence of a population of very compact dwarfs that may have been misclassified as background galaxies in the FCC. Drinkwater et al. (1996) searched unsuccessfully for additional blue compact dwarf (BCD) galaxies in the Virgo Cluster; any compact Virgo cluster galaxies must be fainter than their limit of $b_J = 17.6$. The Fornax cluster has a much lower fraction of late-type dwarfs than Virgo (Ferguson & Sandage 1988), and its core galaxy density is about twice that of Virgo (Ferguson 1989a), offering the chance for an interesting comparison of two dwarf galaxy populations in rather different environments. The initial results of our new spectroscopic survey have already revealed a number of new compact dwarf galaxy members, both early and late types (Drinkwater & Gregg 1998, hereafter Paper I). In this paper we present the rest of our observations with the analysis of a well-defined sample of compact galaxies.

The FCC lists a total of 131 objects as candidate 'M 32-like' compact dwarf ellipticals (cdE). Faber (1973) suggested that high surface brightness, low-luminosity elliptical galaxies (like M 32) are formed by tidal stripping of brighter ellipticals in rich environments, but more recent models find that the amount of mass lost by this process in a Hubble time is too small to produce compact dwarf ellipticals from larger galaxies (Nieto & Prugniel 1987). To test the tidal stripping hypothesis, we observed 97 of the possible cdEs in Fornax to determine if they were cluster members. Whilst there was considerable overlap between these and our compact sample described above, the M 32-like sample also included a number of galaxies with larger scale sizes not included in the compact sample. It should be possible to distinguish galaxies like M 32 from normal dwarf galaxies on the basis of their profiles. We would expect M 32-like bulges to have de Vaucouleurs profiles (Michard & Nieto 1991), whereas most dwarf galaxies have exponential profiles (Ferguson & Binggeli 1994). Our photographic imaging data is not able to resolve differences at this level however, hence the overlap in the two samples. In Paper I we

reported that only one of the M 32 candidates we observed was a cluster member, but that it had an emission-line spectrum inconsistent with a cdE identification. We concluded that tidal stripping had not produced large numbers of cdEs in Fornax (Holman, Drinkwater & Gregg 1995; Drinkwater, Gregg & Holman 1997). In this paper we expand our discussion of the M 32 candidate galaxies in the context of complete samples.

Our measurements of candidate compact cluster galaxies detected a majority of background galaxies, interesting in their own right for large scale structure information. In addition to the new compact cluster members discovered (Paper I), we also observed some 100 known cluster galaxies in order to investigate star formation rates and the dynamics of the cluster, particularly subclustering (Drinkwater, Gregg & Colless 2001, hereafter Paper III). In this paper we adopt a cluster distance of 20 Mpc (Mould et al. 2000, but see discussion in Paper III) corresponding to a distance modulus of 31.5 mag.

In Section 2 we describe how the galaxies were selected and in Section 3 we describe the observations and redshift measurements. We discuss the structure of the cluster in Section 4 and in Section 5 we discuss the star formation process in the dwarf cluster galaxies. The compact dwarf elliptical population is discussed in Section 6 and we summarize all our results in Section 7. We list the background galaxies we observed in the Appendix.

2 SAMPLE SELECTION

The selection criteria for the objects we observed were set by our three overlapping science goals, subject to the capacity of the FLAIR-II spectrograph on the UK Schmidt Telescope of the Anglo-Australian Observatory (Parker & Watson 1995b). This is a multi-object fibre spectrograph with a square field of approximately 6° across. The limiting magnitude of the system is about $b_J = 17.5$ and each observation can take 70 or 90 spectra depending on the plate holder used. It is ideally suited to the
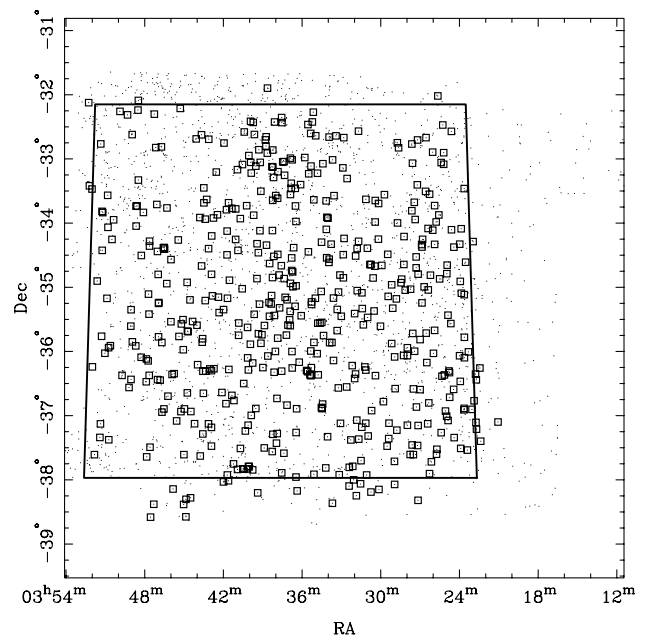

Figure 1. Distribution on the sky of all FCC galaxies (small points), and galaxies observed with FLAIR-II (squares). The region defined by the APM sample is also shown.

---

[1] The NASA/IPAC Extragalactic Database (NED) is operated by the Jet Propulsion Laboratory, California Institute of Technology, under contract with the National Aeronautics and Space Administration.
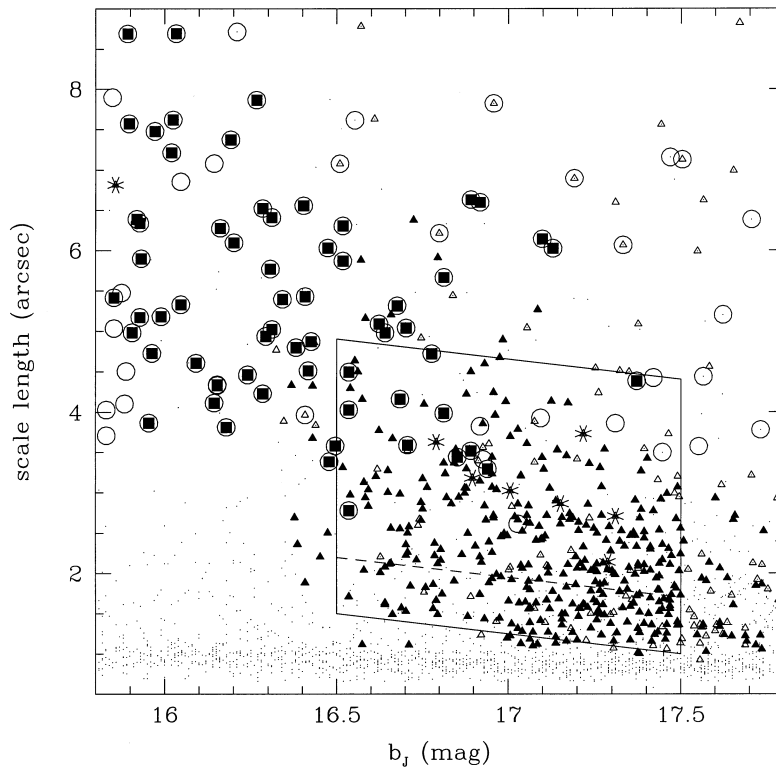
Figure 2. Distribution of b_J magnitudes and scalelength of all resolved objects in the APM catalogue (small points), galaxies observed with FLAIR-II (open triangles; those with redshifts are filled triangles and cluster members are indicated by large filled squares) and galaxies listed as members in the FCC (large circles). New members of the cluster discovered with FLAIR are indicated by asterisks. The parallelogram defines the compact galaxy sample discussed in the text. Objects in the parallelogram above the dashed line form the more conservative sample. Note that for the definitions of these samples, the magnitudes were taken from the APM catalogue, rescaled to approximate the calibrated Davies magnitudes used elsewhere.

measurement of the brighter galaxies in the Fornax cluster which has a core radius of 0.7° (FCC).

Most of our observations were made centred on the standard UK Schmidt sky-survey field termed 'F358' (RA $03^h37^m55\overset{s}{.}9$, Dec. $-34°50'14''$ J2000). As seen in Fig. 1, the cluster is offset from field F358, so some observations were centred on a second field displaced about half a degree south-west (RA $03^h36^m55\overset{s}{.}1$, Dec. $-35°30'11''$ J2000). The overlapping samples we observed are described in the rest of this section.

2.1 Compact galaxies

The primary goal of the project was to search for new cluster compact galaxies, both red and blue, so we concentrated efforts on galaxies with a compact morphology that were *not* classified as cluster members in the FCC. These were selected on the basis of their image parameters measured from the two Schmidt plates described above. Although the targets were initially selected on the basis of compact image morphologies measured from the first Schmidt plate (as described below), many additional targets were later added as the second plate was used and additional 'M 32-like' candidates were included. We can therefore define three different samples of compact galaxies: a statistical sample with defined limits and completeness from a single plate, the list of all M 32 candidates observed and a heterogeneous list of both of these plus any other compact galaxies observed.

The first sample was defined by image parameters measured by the Automatic Plate Measuring (APM) machine, Cambridge, from the UK Schmidt b_J survey plate of field F358. See Irwin, Maddox

& McMahon (1994) for more details of the APM image catalogue. The APM image catalogue lists image positions, magnitudes and morphological classifications (as 'star', 'galaxy', 'noise', or 'merged') measured from both the blue (b_J) and red survey plates. The 'merged' image classification indicates two overlapping images: at the magnitudes of interest for this project, the merged objects nearly always consisted of a star overlapping a much fainter galaxy. The APM magnitudes are calibrated for unresolved (stellar) objects, so for most purposes we use magnitudes estimated by fitting exponential disc profiles to the APM image parameters calculated by Davies et al. (1988) and Irwin et al. (1990) (see Morshidi-Esslinger, Davies & Smith 1999). We refer to these as Davies magnitudes. This process also measures the exponential scalelengths of the images. For galaxies brighter than $b_J = 13$, we have used magnitudes from Ferguson (1989b). There is no evidence for any significant offset between the Davies and FCC magnitudes (Drinkwater et al. 2000b). In one specific case (FCC 39) there seems to be a problem with both the FCC and Davies magnitudes being too faint, so we have adopted the value of $b_J = 13.6$ given by Maddox et al. (1990).

We defined the compact galaxy sample by scalelengths and magnitudes as shown in Fig. 2. To optimize our measurement for the compact objects we used the APM (stellar) magnitudes for this selection, linearly scaled to agree with the Davies magnitudes over this range. The compact galaxy sample is defined in the magnitude range of $16.5 < b_J < 17.5$ by the parallelogram shown in the figure. Basically it includes all galaxies and possible galaxies ('merged' objects) in that magnitude range with sizes smaller than the galaxies classified as cluster members in the FCC. This
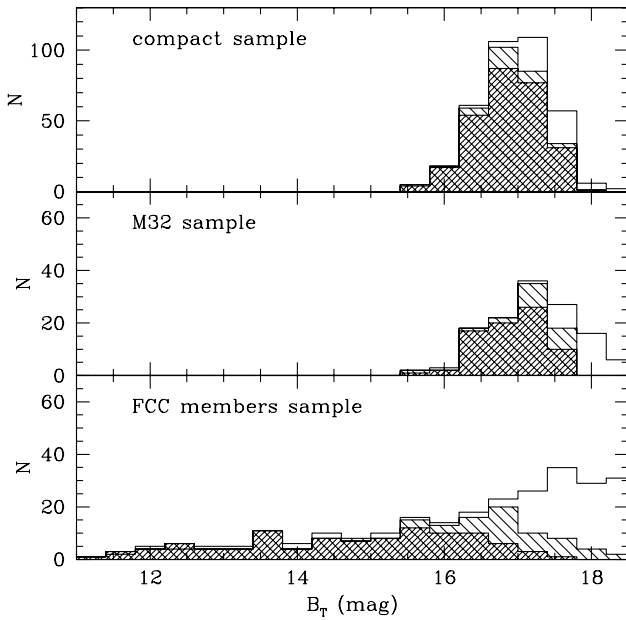
Figure 3. Distributions of B_T magnitudes (from the FCC) of all galaxies from each of the three samples observed: compact galaxies, M 32 candidates from the FCC and definite cluster members from the FCC. In each case the unshaded histogram shows the parent sample, the shaded histogram shows the galaxies observed, and the solid histogram shows those galaxies with measured redshifts. Note the different vertical scale in the top panel.

Table 1. Details of our FLAIR-II observations.

Run	Date	v_{helio} (km s^{-1})	grating
1	1992 October 25	1.4	250B
1	1992 October 26	1.1	250B
2	1993 November 14	−5.3	250B
2	1993 November 15	−5.6	250B
2	1993 November 16	−5.9	250B
3	1994 November 06	−2.7	250B
4	1995 November 22	−7.7	250B
4	1995 November 26	−8.9	250B
5	1996 December 08	−12.5	250B
5	1996 December 09	−12.7	250B
6	1997 October 31	−0.7	600V
6	1997 November 01	−1.0	600V
6	1997 November 08	−3.3	600V

Note: v_{helio} is the correction applied to convert our observed velocities to heliocentric values.

compact subsample consists of 815 objects, of which 25 are FCC members, 400 are FCC background galaxies and the remainder (390) are not listed in the FCC, presumably because they are smaller than the FCC limiting diameter of 17 arcsec. We successfully observed 306, or 38 per cent, of the objects in this sample. Most of the objects not observed were classified as 'merged' and were not measured because they were clearly dominated by a star with visible diffraction spikes. The magnitude distribution of the compact sample is compared with the other samples observed in Fig. 3.

None of the new cluster members were found amongst the smallest objects in the compact sample: these were mostly merged objects dominated by a star. We therefore defined a second, more conservative compact sample by excluding the smallest objects below the dashed line in Fig. 2. This second sample has a higher completeness, comprising 352 compact objects (25 FCC members, 272 FCC background galaxies and 55 not listed in the FCC) of which we measured 211 (60 per cent) to find seven new members.

Our second compact galaxy sample consisted of the 131 galaxies listed in the FCC as possible cdE 'M 32-like' candidates. We observed 97 of these, obtaining 76 reliable redshifts. Fig. 3 shows that these objects were observed to a magnitude limit of $B_T = 17.8$.

Our total compact galaxy sample consisted of the above two samples plus additional compact objects with similar properties. From this sample we measured a total of 437 redshifts.

2.2 Cluster members

We also attempted to observe as many of the cluster members from the FCC as possible in order to have a good sample for studies of the cluster dynamics (Paper III). These were measured with a higher spectral dispersion to give more accurate velocities. The Fornax cluster extends well beyond the limits of a single Schmidt

plate; the FCC includes galaxies in a slightly larger region than defined by our APM sample as is shown in Fig. 1. That figure shows that we observed some galaxies beyond the APM sample. Fig. 3 shows that the member galaxies observed were as faint as $B_T = 18$, but being of generally low surface brightness, the success rate for those fainter than $B_T = 16.6$ was lower than for the other samples.

3 OBSERVATIONS

3.1 Flair-II observations

We observed Fornax for a total of six observing runs. The first five used the low-dispersion 250B grating (coverage 3670–7230 Å, resolution 13 Å), chosen to identify as many galaxies as possible at all redshifts. These observations were severely affected by bad weather, but by the end of the fifth run we had measured most of the compact galaxies within our magnitude limits. For the sixth run we observed FCC-classified members (most of which we had not yet observed) with the medium-dispersion 600V grating (coverage 5150–6680 Å, resolution 5.3 Å), to measure more accurate velocities and study the dynamics of the cluster. A log of our observing runs is shown in Table 1.

3.2 Data reduction and velocity measurement

The data were reduced using the IRAF (Tody 1993) DOFIBERS package. We used the IRAF add-on package RVSAO (Kurtz & Mink 1998) to measure the galaxy redshifts by cross-correlating with template spectra. All velocities were then corrected to heliocentric values using the offsets listed in Table 1.

We checked our velocity errors using measurements of 52 galaxies that were observed twice. The mean and rms values of the velocity differences are shown in Table 2 for the whole sample, and then for two sets of subsamples split according to grating, and also by magnitude. For comparison, we also give the RVSAO estimated mean velocity errors for each sample: these are based on a formal statistical calculation. The results shown in the table are very good, considering the relatively low dispersion and signal-to-noise ratio of our spectra. The velocity resolutions of the 250B and 600V gratings are 650 and 265 km s^{-1} respectively. In particular, the error estimates from RVSAO are shown to be realistic, under-estimating the empirically determined errors by only around 10 per

Table 2. Velocity differences for repeated observations.

sample	N	$\overline{\Delta v}$ (km s^{-1})	$\sigma_{\Delta v}$ (km s^{-1})	$\overline{\sigma_v}$
all	52	10	67	59
600V	9	32	45	44
250B	43	4	69	60
$B_T < 16$	22	26	56	53
$B_T > 16$	30	2	74	62

Notes. $\overline{\Delta v}$ and $\sigma_{\Delta v}$ are the mean and rms velocity differences from repeated observations. For each sample $\overline{\sigma_v}$ is the mean statistical uncertainty based on the RVSAO errors. These rms values are for the difference of two measurements and are $\sqrt{2}$ larger than the rms for a single measurement.

Table 3. Objects with spectra dominated by light from a foreground Galactic star.

RA (J2000) Dec	b_J (mag)	cz (km s^{-1})	Δcz	FCC
03:30:10.12 −33:41:35.8	17.40	193	64	81
03:31:26.86 −37:10:48.5	16.60	41	23	B723
03:33:10.30 −37:55:11.9	17.30	−24	27	B849
03:37:22.01 −34:51:54.1	16.90	86	43	–
03:38:15.18 −34:50:55.2	15.50	39	12	B1239
03:39:19.56 −35:43:28.9	16.80	−5	60	223
03:44:51.01 −38:18:14.0	16.70	−42	34	B1781
03:47:39.18 −36:22:19.3	16.70	74	54	–
03:49:18.67 −32:18:47.3	17.10	99	56	B2112
03:50:48.11 −34:03:58.4	16.10	1	38	–

cent. The improvement with the 600V grating is less than expected, but this is based on a very small number of repeated observations of poor spectra at this dispersion. Note that the rms values discussed here are for the difference of two measurements and are a factor of $\sqrt{2}$ larger than the rms for a single measurement. We have therefore adopted the velocity uncertainties measured by RVSAO.

As a further test of our velocity measurements we compared them to previous measurements in the literature. We found redshift measurements of 102 galaxies in common with our sample in NED (as of 1999 November 23). The mean velocity difference (FLAIR-NED) was $\overline{\Delta v} = -22 \pm 11$ km s^{-1} and $\sigma_{\Delta v} = 108$ km s^{-1}, demonstrating that there were no large systematic errors in our measurements.

In the course of our six observing runs, we observed a total of 675 objects and obtained reliable redshifts for 526 of them. We found that 10 of these objects had absorption-line spectra and velocities consistent with Galactic stars. These were merged objects consisting of a star superimposed on a background galaxy. These were included in the compact sample in case the 'star' was the core of the galaxy, but in each case it was shown to be in the foreground and dominated the spectrum so the background galaxy could not be measured. These objects are listed for reference in Table 3 and are not discussed further in this paper.

Our final sample consists of 108 confirmed cluster galaxies with successfully measured redshifts and is listed in Table 4. The 408 confirmed background galaxies are listed in Table A1. Note that our position for the galaxy FCC 13 is taken from Loveday (1996), as the FCC position is in error.

3.3 Membership status

The full impact of our new measurements is demonstrated in Fig. 4, which gives the distribution of our 516 measured redshifts compared to the 84 redshifts available in the FCC for the same galaxies. The majority of our spectra are of background galaxies, as expected because our aim was to search for new cluster members among galaxies classified as 'background' in the FCC. The membership classifications of the objects we observed are compared to the FCC classifications in Table 5. As in Paper I, we detect a clear void behind the Fornax cluster, with no galaxies having redshifts between 2320 and 4180 km s^{-1}, so we define any galaxy with a redshift less than 3000 km s^{-1} as a member of the cluster.

We find that the FCC membership classifications were very reliable: out of 516 galaxies measured, only nine were members misclassified as background galaxies in the FCC and only three were background galaxies misclassified as members. These 12 objects with new membership classifications are listed in Table 6. Note that one additional new cluster member (FCC B1241) was reported in Paper I. Although this galaxy was in our FLAIR-II sample, it was not observed successfully with FLAIR-II (the identification was from 2dF observations), so shall not be discussed in this current paper.

The properties of the new cluster members are discussed in detail below. Six of these were first presented in Paper I; our present analysis has produced an additional three new cluster members. We also found three background galaxies that were classified as members in the FCC; these include two of the FCC candidate late-type dwarf galaxies (FCC 24 and FCC 123). These both had emission-line spectra confirming the late-type classification if not the membership. We inspected images of all the re-classified objects by eye on the b_J survey plates and there was no apparent reason why they should not have been given the FCC classifications. This only goes to emphasize the limitations of the morphological classification.

More interestingly, our sample of compact galaxies drawn from the APM data included 10 objects not in the FCC: three of these were objects dominated by the light from foreground stars (Table 3), but seven are background galaxies, listed in Table 7. These were not included in the FCC because of their very compact appearance; the FCC is diameter-limited at 17 arcsec, while these objects have scalelengths of 2 arcsec or less. Only one has been previously measured (APMBGC 359+114+047) as part of the Stromlo/APM galaxy redshift survey (Loveday et al. 1996); the others we give new names in Table 7 according to the IAU-approved convention for our larger Fornax Cluster Spectroscopic Survey (Drinkwater et al. 2000b).

We can use the statistical samples defined in Fig. 2 to put limits on the total number of new compact cluster members. In the upper region in the figure (above the dashed line) we found seven new members, having observed 327 galaxies not listed as members in the FCC; the probability of getting a new member is therefore $p \approx (7/327) = 0.02$. Using this as a binomial probability, the expected number of new members among the remaining 141 galaxies we didn't observe in this region is therefore equal to three, and the 98 per cent upper limit on the additional new members is equal to seven. There is clearly no large population of new members still to be found in this magnitude range.

3.4 Spectroscopic classification

Our spectroscopic data not only allow us to confirm the cluster

Table 4. Catalogue of all Fornax Cluster members with redshifts measured with FLAIR-II.

FCC	RA (J2000) Dec	cz (km s^{-1})	σ_{cz}	EW(Hα)(Å)	T-type	b_J (mag)	SB (mag arcsec^{-2})	α (arcsec)	P1(1)
13	03:21:03.7 −37:05:58	1792	25	11.8	5	12.0	–	–	0.01
19	03:22:22.9 −37:23:50	1497	47	−0.7	−5	15.2	–	–	0.01
21	03:22:42.2 −37:12:36	1659	17	1.0	−1	09.4	–	–	0.01
22	03:22:44.6 −37:06:16	1980	18	15.4	1	11.9	–	–	0.01
26	03:23:37.3 −35:46:43	1718	46	3.5	−1	16.4	22.3	6.1	0.18
28	03:23:54.3 −37:30:33	1381	28	9.3	9	13.5	18.4	3.9	0.02
29	03:23:56.3 −36:27:57	1244	19	18.6	1	11.8	–	–	0.01
32	03:24:52.5 −35:26:08	1318	26	9.6	−5	16.1	21.8	5.4	0.17
33	03:24:58.5 −37:00:34	1994	19	4.0	7	14.2	21.4	6.3	0.02
35	03:25:04.1 −36:55:40	1797	15	175	9	16.1	21.3	4.2	0.02
37	03:25:09.1 −36:21:55	1785	59	3.8	5	13.8	21.8	7.1	0.04
36	03:25:12.2 −32:54:10	2325	90	1.3	−5	16.2	21.2	4.0	1.00
39	03:25:19.8 −36:23:05	991	13	23.3	7	13.6	21.6	6.1	0.02
43	03:26:02.5 −32:53:42	1323	17	−1.7	−5	15.1	21.6	7.6	1.00
46	03:26:25.1 −37:07:39	2220	32	2.1	−5	16.5	21.3	3.6	0.06
47	03:26:32.1 −35:42:49	1473	23	−0.6	−4	13.3	21.3	8.7	0.18
55	03:27:18.1 −34:31:34	1279	17	−0.8	−1	15.5	20.6	4.1	0.95
B 470	03:27:33.8 −35:43:04	723	79	0.3	0	17.5	21.1	2.1	0.12
62	03:27:58.3 −37:08:57	1813	13	61.6	4	12.6	15.9	3.7	0.46
67	03:28:48.8 −35:10:49	1345	44	2.8	5	14.2	21.1	5.5	0.85
76	03:29:43.4 −33:33:26	1808	14	6.1	10	16.3	22.3	6.4	1.00
83	03:30:35.2 −34:51:19	1477	11	0.4	−4	12.3	–	–	1.00
88	03:31:08.1 −33:37:47	1924	15	0.1	3	11.8	–	–	1.00
90	03:31:08.2 −36:17:24	1813	15	11.2	−4	15.6	21.8	6.9	1.00
95	03:31:24.8 −35:19:51	1275	26	−0.5	−1	15.2	20.4	4.3	1.00
B 729	03:31:32.5 −38:03:43	1676	31	6.8	−5	16.5	–	–	1.00
100	03:31:47.7 −35:03:05	1660	31	−0.4	−5	15.9	22.4	7.9	1.00
102	03:32:10.8 −36:13:13	1723	61	13.0	10	16.8	22.2	5.0	1.00
106	03:32:47.8 −34:14:19	2064	35	−1.4	−1	16.3	22.3	6.3	1.00
113	03:33:06.8 −34:48:32	1365	23	10.1	5	15.5	22.2	8.7	1.00
119	03:33:33.9 −33:34:23	1384	40	−0.1	−1	15.7	21.2	5.0	1.00
121	03:33:36.3 −36:08:28	1446	12	43.5	4	10.2	–	–	1.00
B 904	03:33:56.2 −34:33:43	2254	56	−0.1	−5	17.4	21.7	2.9	1.00
B 905	03:33:57.2 −34:36:43	1242	23	18.2	10	17.7	22.5	3.7	1.00
136	03:34:29.5 −35:32:46	1217	24	−1.1	−5	16.3	21.6	4.8	1.00
135	03:34:30.9 −34:17:51	1381	49	−0.5	−5	16.5	22.3	5.8	1.00
139	03:34:57.4 −32:38:22	1752	24	13.6	9	15.3	20.2	3.8	1.00
143	03:34:59.2 −35:10:15	1364	16	−1.1	−4	14.5	20.9	7.6	1.00
147	03:35:16.9 −35:13:39	1299	17	−0.8	−4	12.0	–	–	1.00
148	03:35:16.9 −35:16:01	794	17	−1.3	−1	13.9	19.4	5.0	1.00
B 1005	03:35:20.4 −32:36:08	1256	36	−0.2	−1	13.7	19.9	6.8	1.00
150	03:35:24.1 −36:21:49	2031	26	−1.1	−5	16.2	21.4	4.5	1.00
153	03:35:31.1 −34:26:49	1589	10	−0.7	−1	14.2	19.2	4.1	1.00
152	03:35:33.2 −32:27:50	1389	12	7.4	0	14.9	20.7	5.9	1.00
161	03:36:04.1 −35:26:34	1342	16	−1.4	−4	12.6	–	–	1.00
164	03:36:12.9 −36:09:59	1430	33	−1.9	−5	17.0	22.1	4.2	1.00
167	03:36:27.6 −34:58:36	1953	13	0.1	0	11.3	–	–	1.00
170	03:36:31.7 −35:17:48	1763	14	−0.7	−1	12.5	17.5	4.0	1.00
176	03:36:45.1 −36:15:22	1399	30	−1.1	1	13.7	21.4	9.6	1.00
174	03:36:45.4 −33:00:49	1645	78	−1.2	−5	16.8	21.8	4.0	1.00
179	03:36:46.4 −36:00:02	972	17	4.5	1	12.4	–	–	1.00
177	03:36:47.5 −34:44:22	1622	21	−0.3	−1	13.2	20.3	5.4	1.00
B 1108	03:36:49.7 −33:27:39	1734	137	−0.1	−5	17.8	22.5	3.6	1.00
181	03:36:53.2 −34:56:17	1113	53	−0.2	−5	17.7	22.9	4.4	1.00
182	03:36:54.4 −35:22:27	1657	19	−1.6	−1	15.0	21.3	7.2	1.00
184	03:36:57.0 −35:30:29	1257	12	0.1	−1	12.3	–	–	1.00
188	03:37:04.6 −35:35:24	1004	80	−1.6	−5	16.1	22.1	6.3	1.00
190	03:37:09.0 −35:11:42	1740	17	−1.2	−1	13.5	20.1	6.4	1.00
193	03:37:11.8 −35:44:44	921	12	−1.1	−1	13.2	–	–	1.00
201	03:37:53.7 −37:16:47	1922	126	0.7	−5	17.3	23.2	6.0	1.00
202	03:38:06.6 −35:26:23	808	22	−0.7	−4	16.1	21.5	4.9	1.00
203	03:38:09.3 −34:31:06	1173	30	−0.6	−5	16.8	22.1	4.5	1.00
206	03:38:13.5 −37:17:23	1402	20	14.4	−5	16.9	22.9	6.1	1.00
204	03:38:13.8 −33:07:36	1369	28	−0.5	−5	15.8	21.4	5.3	1.00
207	03:38:19.3 −35:07:43	1419	43	2.2	−5	16.1	21.5	4.9	1.00
211	03:38:21.5 −35:15:35	2276	23	−0.1	−4	16.8	21.6	3.6	1.00
213	03:38:29.3 −35:27:07	1433	26	0.1	−4	10.6	–	–	1.00
219	03:38:52.2 −35:35:42	1897	21	−0.2	−4	10.0	–	–	1.00
B 1379	03:39:55.0 −33:03:09	745	21	17.3	−5	17.3	21.7	3.0	1.00
235	03:40:09.3 −35:37:28	1974	20	23.1	10	13.4	22.1	7.3	1.00
243	03:40:27.0 −36:29:56	1404	52	−2.8	−5	16.7	22.5	5.7	1.00

Table 4 – *continued*

FCC	RA (J2000) Dec	cz (km s^{-1})	σ_{cz}	EW(Hα)(Å)	T-type	b_J (mag)	SB (mag arcsec^{-2})	α (arcsec)	P1(1)
245	03:40:33.8 −35:01:21	2124	68	−1.1	−5	16.6	22.7	6.6	1.00
249	03:40:42.1 −37:30:38	1571	18	−0.6	−4	14.1	19.7	5.2	1.00
252	03:40:50.4 −35:44:53	1415	35	−1.9	−5	16.1	22.0	6.0	1.00
253	03:40:55.2 −37:50:16	1677	57	−2.0	−5	17.0	22.4	4.7	1.00
255	03:41:03.5 −33:46:43	1283	25	−1.0	−1	13.9	19.2	4.5	1.00
261	03:41:21.5 −33:46:09	1492	42	4.5	−5	16.7	22.3	5.3	1.00
263	03:41:32.3 −34:53:22	1691	15	32.9	6	14.9	20.2	4.7	1.00
266	03:41:41.3 −35:10:12	1551	39	−1.3	−5	16.0	20.7	3.4	1.00
267	03:41:45.6 −33:47:29	834	10	13.4	9	16.4	22.3	5.9	1.00
B 1554	03:41:59.5 −35:20:53	1642	52	−0.8	−4	17.7	21.8	2.7	1.00
276	03:42:19.3 −35:23:41	1382	12	−0.8	−4	12.6	–	–	1.00
277	03:42:22.8 −35:09:15	1613	25	−0.4	−4	13.9	20.0	5.0	1.00
278	03:42:27.3 −33:52:14	2125	30	−1.2	−5	17.4	22.1	3.5	1.00
282	03:42:45.6 −33:55:12	1267	36	8.2	10	15.0	20.1	4.3	1.00
285	03:43:01.9 −36:16:16	891	6	22.8	7	14.2	22.5	9.3	1.00
288	03:43:22.8 −33:56:20	1103	37	−1.7	−5	16.8	22.0	4.5	1.00
290	03:43:37.1 −35:51:17	1392	20	−0.4	5	12.4	–	–	1.00
296	03:44:32.9 −35:11:45	816	122	−0.9	−5	16.7	22.3	5.0	1.00
298	03:44:44.4 −35:41:01	1719	36	−1.1	−5	17.1	21.7	3.4	1.00
299	03:44:58.6 −36:53:42	2151	40	29.7	7	17.9	22.5	3.3	1.00
301	03:45:03.6 −35:58:22	1005	19	−0.9	−4	14.6	20.2	5.2	1.00
302	03:45:12.3 −35:34:14	806	23	20.2	8	17.1	23.2	6.5	1.00
303	03:45:14.1 −36:56:12	1980	31	−2.9	−5	15.5	21.9	7.4	1.00
305	03:45:33.8 −37:04:58	1228	25	−1.2	−5	16.8	22.3	5.1	1.00
306	03:45:45.4 −36:20:45	898	14	34.7	9	16.1	20.4	2.8	1.00
308	03:45:54.9 −36:21:30	1484	25	16.3	7	13.8	22.3	7.5	1.00
310	03:46:13.8 −36:41:48	1373	13	−1.0	−1	14.0	20.5	7.9	1.00
312	03:46:19.0 −34:56:36	1898	22	22.5	5	13.5	–	–	1.00
316	03:47:01.4 −36:26:15	1546	105	−0.4	−5	16.9	23.0	6.6	1.00
315	03:47:04.7 −33:42:34	1071	15	−0.1	2	12.6	–	–	1.00
319	03:47:16.1 −32:18:08	1445	61	−0.1	−5	17.1	23.1	6.6	1.00
322	03:47:33.2 −38:34:54	978	15	54.4	7	12.5	–	–	1.00
324	03:47:52.8 −36:28:18	1493	44	−1.1	−5	16.7	22.4	5.4	1.00
B 2144	03:49:53.3 −32:15:33	1184	25	65.1	−4	17.1	21.6	3.2	1.00
335	03:50:36.8 −35:54:34	1367	24	−0.1	−4	15.2	20.5	4.6	1.00
336	03:50:52.6 −35:10:19	1956	67	0.4	−5	18.0	22.7	3.4	1.00
338	03:52:01.1 −33:28:07	1562	16	32.9	−1	14.3	–	–	1.00

Note: (1) P1 is the probability that the galaxy lies in the Fornax-main cluster and not the Fornax-SW subcluster.

membership of the Fornax galaxies, but they also give us the opportunity to revise the classifications of individual cluster members on the basis of measured spectral indicators of star formation. The FCC galaxies were given morphological classifications in the extended Hubble system following the work by Sandage (see FCC). For the purpose of our current analysis we have converted these classifications to a one-dimensional sequence of 'revised morphological types' or 't-types' following de Vaucouleurs et al. (1991, hereafter RC3). The correspondences between the FCC types and the t-types we have used are given in Table 8, which is based on Table 2 of the RC3 galaxy catalogue, except for the early-type dwarfs which are not defined in that table. We assigned dE and dS0 galaxies a t-type of −5, based on the classification of some dwarf galaxies in the Local Group. To the one cluster member classified as '?' we assigned a value of 10 (Im).

The one line that is detectable in all our spectra is the Hα emission line. We measured Hα equivalent widths interactively using the IRAF task SPLOT, defining the continuum level from regions both sides of the Hα line, avoiding the [N II] lines. In Fig. 5 we plot the equivalent widths of Hα as a function of the newly assigned galaxy t-types; the Hα equivalent widths are listed in Table 4. There is a general correlation: most of the late-classified galaxies show emission lines and the dE/dS0 galaxies mostly have low equivalent widths of Hα. However, several of the early-type

galaxies do have significant emission in Hα, notably the new cluster member FCCB 2144 with an equivalent width of 65 Å that was previously classified as 'E or dE(M 32)'. Our 3σ detection for Hα emission corresponds to an equivalent width of 1.0 Å. We classify the 42 galaxies with Hα emission above this limit as late types and the remainder (66) as early types.

The new spectroscopic classifications reveal a much higher incidence of star-forming dwarf galaxies in the cluster than is implied by the original morphological classifications, as summarized in Table 9. This trend is discussed further in Section 5.1 where we also consider the effect of any bias on the new classifications caused by the limited aperture size of our observations. It is clear that reliable morphological classifications would need higher resolution and/or dynamic range material than a wide-field photographic plate, i.e. the FCC classifications were influenced by the data characteristics as noted by Ferguson at the time.

4 CLUSTER STRUCTURE

The 108 confirmed cluster galaxies we have measured constitute a very useful sample to examine the structure of the cluster as they were uniformly selected over a very large field. This is also the first spectroscopic sample of cluster galaxies to contain a significant
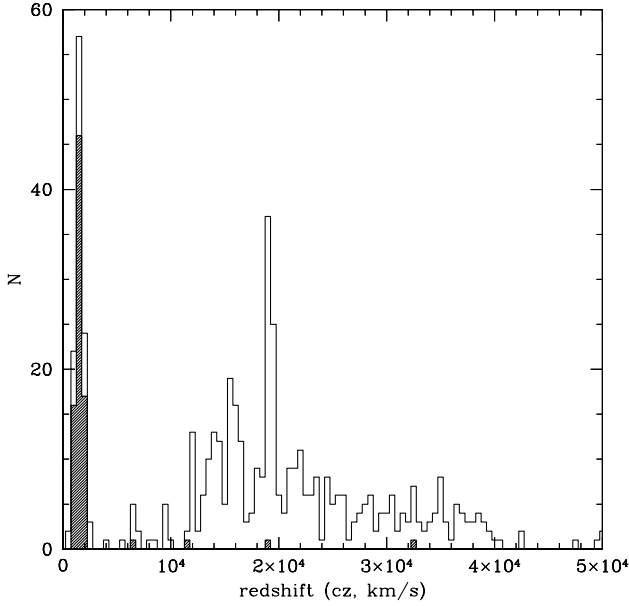
Figure 4. Distribution of the 516 galaxy velocities measured for this work (unshaded histogram) compared to the 84 measurements for the same galaxies in the FCC (shaded histogram).

Table 5. Comparison of new spectroscopic classification with FCC membership classes.

FLAIR-II classification	star	member	background	total
FCC member	2	99	3	104
FCC background	5	9	398	412
not in FCC	3	–	7	10
total	10	108	408	526

Table 6. Galaxies listed in the FCC with changed membership classifications.

RA (J2000) Dec	b_J	cz (km s^{-1})	Δcz	FCC	type
03:23:31.7 −34:36:34	15.2	13222	14	24	BCD
03:27:33.8 −35:43:04	17.5	723	79	B470	S/Im
03:31:32.5 −38:03:43	16.5	1676	31	B729	(d)S0
03:33:43.4 −35:51:33	17.9	15483	60	123	ImV
03:33:56.2 −34:33:43	17.4	2254	56	B904	(d)E
03:33:57.2 −34:36:43	17.7	1242	23	B905	?
03:35:20.4 −32:36:08	13.7	1256	36	B1005	S0
03:36:49.7 −33:27:39	17.8	1734	137	B1108	(d)S0
03:39:55.0 −33:03:09	17.3	745	21	B1379	dE
03:41:59.5 −35:20:53	17.7	1642	52	B1554	E
03:46:18.2 −33:45:48	17.9	47658	60	311	dS0
03:49:53.3 −32:15:33	17.1	1184	25	B2144	(d)E

Note: the final column ('type') gives the FCC morphological classification.

fraction of dwarf galaxies. For the purposes of this paper we define dwarf galaxies to be those with $b_J \geq 15$ ($M_B \geq -16.5$) in our sample. This is slightly brighter than we have used elsewhere ($b_J \geq 15.5$ in Paper III) so as to give a larger sample (62 dwarfs) for our analysis, but there is a natural break in the luminosity distribution at this limit and it matches the luminosity of the brightest Local Group dwarfs (Mateo 1998). Our analysis of the galaxy velocities has revealed the first significant evidence for

Table 7. Background galaxies not listed in the FCC.

Name	RA (J2000) Dec	cz (km s^{-1})	Δcz
FCSS J032700.2−354854	03:27:00.2 −35:48:55	25548	44
FCSS J033154.8−343045	03:31:54.9 −34:30:45	21972	33
FCSS J033744.9−344834	03:37:45.0 −34:48:34	26232	133
FCSS J033757.0−372542	03:37:57.1 −37:25:43	16923	31
FCSS J034111.5−364550	03:41:11.5 −36:45:50	31302	36
APMBGC 359+114+047	03:51:17.1 −35:45:49	18102	51
FCSS J035159.5−361420	03:51:59.5 −36:14:20	14505	34

Table 8. Correspondence between new galaxy 't-types' adopted and FCC classifications.

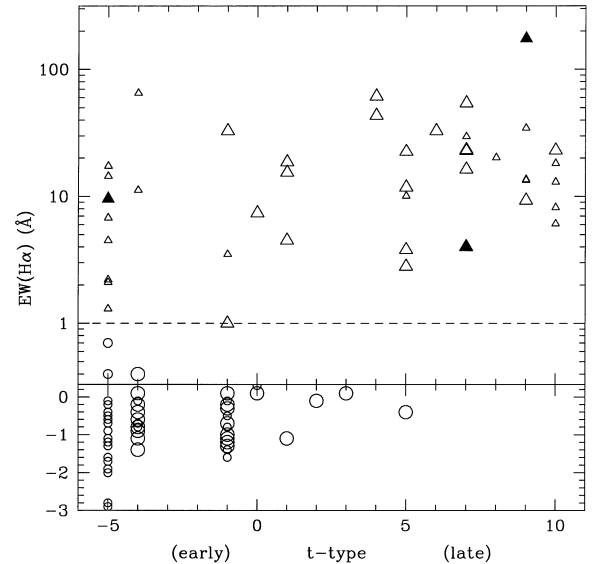| t-type	FCC type	t-type	FCC type
−5	dS0, dE	5	Sc, SBc
−4	E	6	Scd, SBcd
−1	S0, SB0	7	Sd, SBd
0	S0/a, S, SB	8	Sdm
1	Sa, SBa, RSa	9	Sm, SBm
2	Sab, SBab	10	Im, BCD, ?
3	Sb, SBb	15	other
4	Sbc, SBbc	20	unclassified

Figure 5. Equivalent widths of Hα emission as a function of morphological t-types of 108 Fornax cluster galaxies. The equivalent widths are measured from our FLAIR-II spectra with positive values indicating emission. The t-types are derived from the FCC morphological classifications as discussed in the text. Galaxies with widths greater than our 3σ detection limit of 1 Å (indicated by the dashed line) are plotted as triangles and the rest as circles with the larger symbols in each case for the giant galaxies. The three galaxies with possible BCD classifications are indicated by filled triangles. The scale is logarithmic for widths greater than our 1σ limit of 0.3 Å (indicated by the horizontal axis) and linear for smaller values.

substructure in the Fornax Cluster. This is presented fully in Paper III, so we only summarize it in this section.

4.1 Cluster membership

The overall distribution of the cluster members is shown in Fig. 6 as cone diagrams in right ascension and declination. The figure

shows all objects measured between velocities of zero and 7000 km s^{-1}, to emphasize the clear demarcation between the cluster and foreground stars on the one hand and background galaxies on the other. The figure also differentiates between early- and late-type cluster members as discussed in the next section. The locations of the nine new cluster members are indicated by circles; their positions are not significantly different to those of the previously classified cluster members.

Our new measurements represent a large increase in the number of confirmed dwarf galaxies in the Fornax Cluster, from 26 with redshifts in the FCC to 62 in our sample. However, as only nine of our sample were not already classified as cluster members in the FCC, this does not represent a significant change in the cluster luminosity function. At fainter levels ($b_J > 18$, $M_B > -13.5$) the galaxy counts in the FCC tail off rapidly so it is presumably incomplete.

4.2 Substructure and dynamics

We present histograms of the velocity distributions of cluster galaxies and various subsamples in Fig. 7. The total cluster sample has a marginally non-Gaussian velocity distribution at the 91 per cent confidence level using the W-test (Royston 1982). The mean velocity is 1493 ± 36 km s^{-1} and the velocity dispersion is 374 ± 26 km s^{-1}.

The other subsamples (late and early types; dwarfs and giants as defined in Section 3) are all consistent with Gaussian distributions. There is however an indication in Fig. 7 of differences in the velocity dispersions of the subsamples. The velocity dispersion of

the dwarfs (409 ± 37 km s^{-1}) is larger than that of the giants (324 ± 34 km s^{-1}) at the 90 per cent confidence level as measured by the F-test (Press et al. 1992). The larger velocity dispersion of the dwarfs, combined with their more extended spatial distribution (Section 4.3) suggests that they are infalling, whereas the giants form a virialized population (see Paper III). The dispersions of the late-type (405 ± 45 km s^{-1}) and early-type samples (356 ± 31 km s^{-1}) are not significantly different.

In Paper III we describe in detail the evidence for substructure in this galaxy distribution. We used a mixture modelling algorithm as described by Colless & Dunn (1996) to identify a robust partition of the cluster into a 92-member main cluster, centred close to NGC 1399 with $\overline{cz} = 1478$ km s^{-1} and $\sigma_{cz} = 370$ km s^{-1}, and a 16-member subcluster, centred about 3 degrees to the south-west (SW) with $\overline{cz} = 1583$ km s^{-1} and $\sigma_{cz} = 377$ km s^{-1}. The partition is indicated in Table 4 in the form of a probability for each cluster member that it is a member of the main cluster. Note that the subcluster does not contain the giant barred spiral NGC 1365 which is closer to the centre of the field, but it does contain the active radio galaxy Fornax A (NGC 1316) as well as a high concentration of other late-type galaxies. The two-sigma limits of the cluster and subcluster are shown in Fig. 8. A simple two-body dynamical model allows for solutions with the subcluster either in front of the main cluster (infalling) or behind the main cluster (moving away), but the infalling solution is slightly more probable. We use these dynamical data in Paper III to make new estimates of the cluster mass using both virial mass estimators and the velocity amplitude method of Diaferio (1999). The cluster mass within a projected radius of 1.4 Mpc is $(7 \pm 2) \times 10^{13}$ M$_\odot$, corresponding to a mass-to-light ratio of 300 ± 100 M$_\odot$/L$_\odot$.

4.3 Spatial distribution

The projected galaxy distribution in Fig. 8 shows evidence that the late-type galaxies are more widely distributed than the early types. This is confirmed in Fig. 9, which is a plot of the normalized cumulative radial distributions for different galaxy subsamples. Note that for this radial analysis we restrict our analysis to the 92 members of the main cluster. Even after the removal of the SW subcluster which is dominated by late-type galaxies, the late-type galaxy subsample is significantly more extended than the rest of
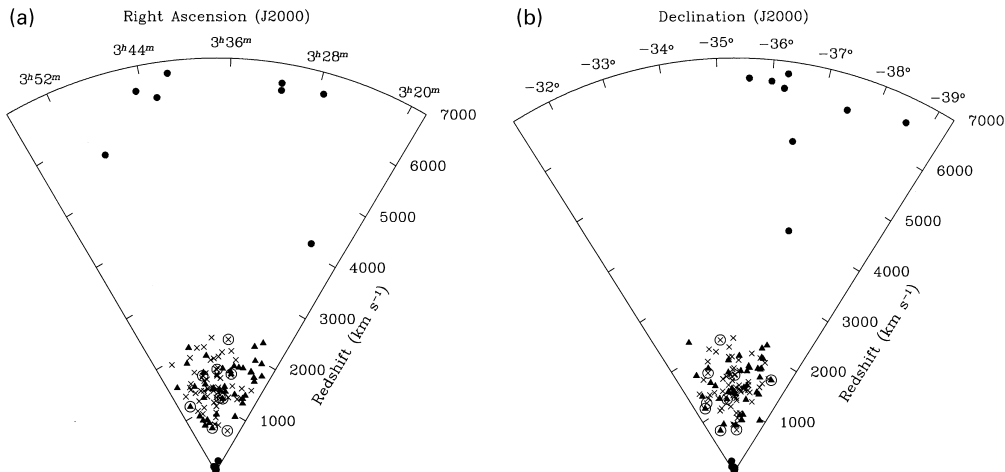
Table 9. Comparison of new spectroscopic classifications with FCC morphological types. The dwarf sample is defined as galaxies with $b_J \geq 15.0$.

Sample	FCC type	N	Spectroscopic type	
			absorption	emission
dwarf	early	50	39	11
dwarf	late	12	1	11
giant	early	23	21	2
giant	late	23	5	18
total	–	108	66	42

Figure 6. Distribution of cluster galaxies. Cluster members are indicated as early types (crosses), late types (triangles) and new members (additional circles). Solid circles indicate foreground stars and background galaxies.
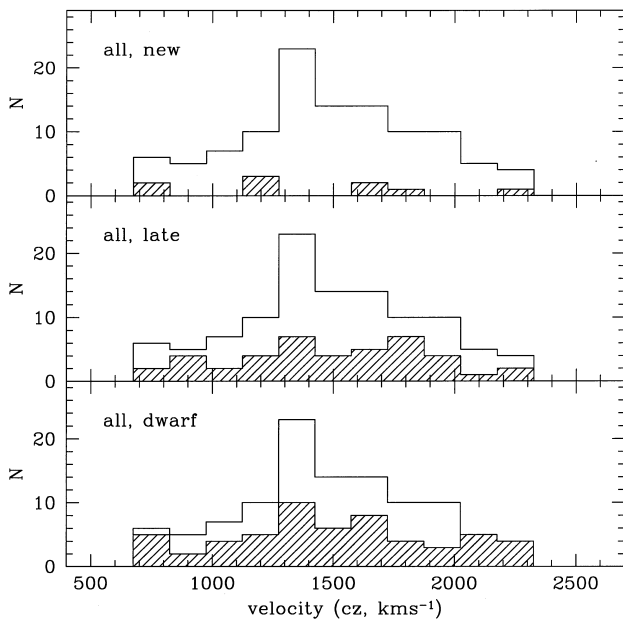
Figure 7. Histograms of Fornax Cluster galaxy velocities. In each panel the unshaded histogram shows the full sample of 108 galaxies. The shaded histograms show various subsets: the nine new cluster members (top panel), the 42 late-type galaxies (middle) and the 56 dwarf galaxies (bottom panel).
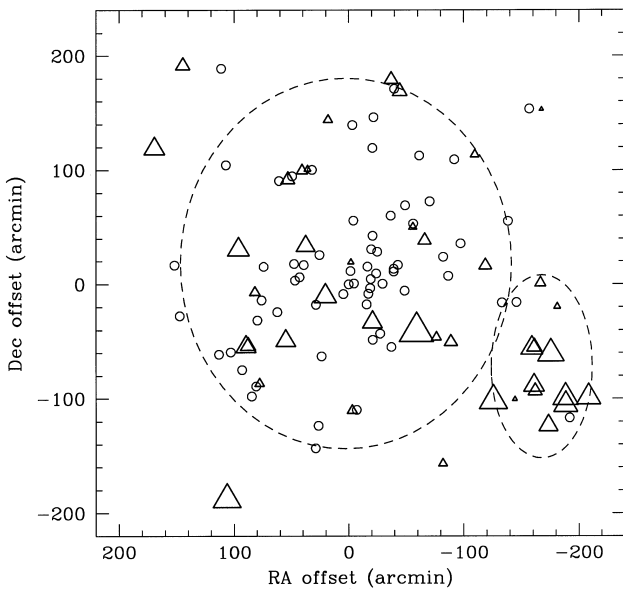

Figure 8. Projected spatial distribution of Fornax cluster galaxies. Galaxies spectroscopically classified as early type are plotted as circles and late types as triangles. The symbol sizes of the late-type galaxies are scaled by the logarithm of their star formation rates (ranging from 10^{-3} to $6\,M_{\odot}\,y^{-1}$) derived from their magnitudes and Hα equivalent widths as described in Section 5.3. The dashed ellipses show the 2-sigma limits of the two subclusters.

the cluster galaxies. The two distributions differ at the 99 per cent confidence level measured by the Kolmogorov–Smirnov (KS) test. The dwarf galaxies are also more extended than the giant galaxies (middle panel of Fig. 9) at the 99 per cent confidence level. Restricting the analysis to the dwarf galaxies alone (lower panel of Fig. 9), the fraction of late-type dwarfs also decreases towards the
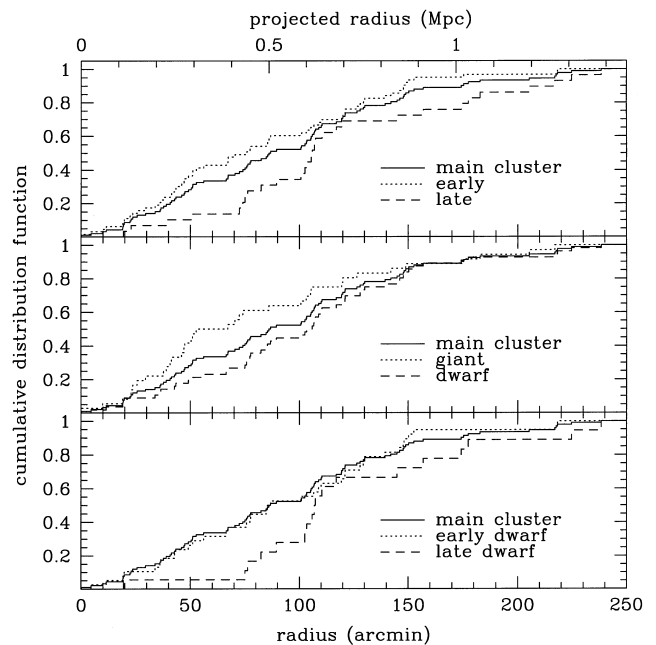
Figure 9. Cumulative radial distributions of various galaxy samples in the 92-member main part of the Fornax Cluster. In each plot the total distribution is shown as a solid line. These are compared to the early (dotted) and late-type (dashed) subsamples (upper panel), the dwarf (dotted) and giant (dashed) subsamples (middle panel) and the dwarf early- (dotted) and dwarf late- (dashed) type subsamples (lower panel).

cluster centre, but given the smaller sample (56 dwarfs) the difference is only at the 85 per cent confidence level.

5 STAR FORMATION IN DWARF GALAXIES

5.1 New star-forming galaxies

As described above, we reclassified the measured Fornax Cluster galaxies as late or early types from their spectroscopic properties, independent of their morphologies. This spectral reclassification is based on our FLAIR-II data, i.e. spectra taken through 6.7-arcsec fibres centred on the individual galaxies. We therefore need to consider how representative the spectra are of the whole galaxies, especially as star formation is often centrally concentrated in dwarf galaxies. Gallagher & Hunter (1989) obtained Hα imaging and spectroscopy for a sample of about 30 Virgo Cluster dwarf irregulars. They found that the Hα emission was significantly centrally concentrated in 30 per cent of their sample. In the remaining galaxies, the distribution of Hα emission followed that of the red continuum light, in which case central measurements of the Hα equivalent width would be representative of the whole galaxy. A spectroscopic analysis of the nuclei of Fornax dwarf galaxies (Held & Mould 1994) found evidence for young stellar populations in some of them. Our sample includes two of the same galaxies (FCC 207 and 261) in which we detected weak Hα emission. Held & Mould (1994) remarked that FCC 207 is blue in $U - B$ colour, indicating a young population, although their spectra did not extend far enough into the red to allow them to detect the Hα emission.

Ideally we would avoid any bias by classifying galaxies as a function of their *total* Hα emission, normalized in some way by the galaxy size or mass. The measurement of Hα equivalent width (EW) is one example of this normalization. The only reliable way
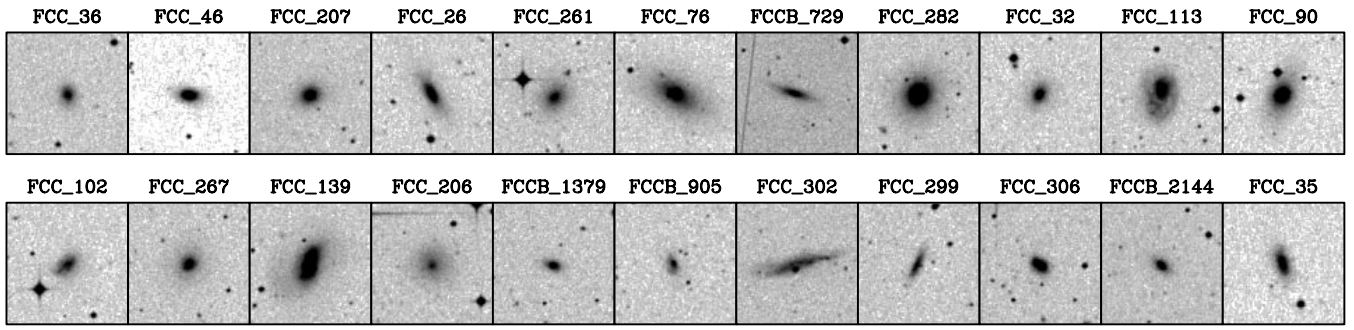
FCC_36	FCC_46	FCC_207	FCC_26	FCC_261	FCC_76	FCCB_729	FCC_282	FCC_32	FCC_113	FCC_90

FCC_102	FCC_267	FCC_139	FCC_206	FCCB_1379	FCCB_905	FCC_302	FCC_299	FCC_306	FCCB_2144	FCC_35

Figure 10. Fornax cluster dwarf galaxies showing significant star formation plotted in order of increasing Hα equivalent widths from left-to-right and top-to-bottom. The two galaxies previously classified as BCDs are FCC 32 and FCC 35. These Digitized Sky Survey (DSS) blue optical images are each about 3 arcmin across.

to measure the total Hα emission is with large-aperture spectroscopy or narrow-band Hα imaging. This is not available for our sample, although we plan to obtain Hα images of these galaxies in the future. If the Hα emission were centrally concentrated, then our EW measurements would over-estimate the average values for each galaxy. We can estimate a lower limit for the total EW by considering an extreme case where all the emission is in the central region. The total EW is then just our measured value multiplied by the fraction of the total galaxy (continuum) light sampled by the aperture of the spectrograph. The effective aperture of the FLAIR-II system is a convolution of the 6.7-arcsec fibre diameter with image movement during the observation (caused by tracking errors and differential atmospheric refraction). These errors are difficult to quantify (Parker & Watson 1995a), but the image translation during long exposures is at least as large as the fibre apertures, because we have observed significant flux variations between different targets between exposures. The effective aperture is therefore at least 15 arcsec in diameter. To calculate the fraction of light observed for each galaxy, we use the exponential scalelengths already measured from the APM data (shown in Fig. 11) and an aperture radius of 8 arcsec. For a dwarf with scalelength of 4 arcsec this implies we have observed 60 per cent of the light and that the lower limit of the total EW is 60 per cent of that measured in our spectra.

We estimated lower limits of total EW for all 11 dwarfs which we had reclassified as late type: only one of them resulted in a value lower than our 1-Å cutoff: FCC 36 originally classified as 'dE4 pec,N' in the FCC. So, although our FLAIR-II spectra are biased towards light from the galaxy cores (around 8 arcsec or 800 pc in radius), the detections are strong enough that they would have a significant detection of Hα emission when averaged over the whole galaxy. We are therefore confident in our use of spectral classifications, although Hα imaging will give us more accurate numbers in the future.

Our spectral reclassification results in a higher fraction of late-type galaxies than implied by morphological classification, especially for the dwarfs (see Table 9). Of the 62 dwarfs measured, 12 were morphologically classified as late type in the FCC ($t \geq 0$), but we find that twice this number (22) have detected Hα emission. The fraction of late-type dwarfs in our sample is therefore 35 per cent, compared to 19 per cent using the FCC classifications. For the total cluster sample in the FCC, the fraction (Im types compared to dE + dS0 + Im) is 13 per cent. We compared the properties of the 11 newly identified star-forming dwarfs with the other cluster galaxies. Their radial and velocity distributions are not significantly

different to the other galaxies, but we note that their Hα equivalent widths are significantly lower at a KS significance of 94 per cent. As might be expected, it is the dwarfs with lower star formation rates that were not identified by morphology in the FCC. The exception to this is the high star formation galaxies which were previously misclassified as background objects (see Paper I).

We show b_J images of all 22 star-forming dwarf galaxies in Fig. 10 in order of increasing Hα equivalent width. The low equivalent width dwarfs do resemble dE types, but we do not identify any significant difference in the measured morphological parameters scalelength and magnitude between the old and new star-forming dwarfs. The new star-forming dwarfs have a slightly brighter mean surface brightness, but the difference is only significant at the 84 per cent level.

5.2 Blue compact dwarf galaxies

Blue compact dwarfs (BCDs) are defined as high surface brightness, compact, star-forming dwarf galaxies (Thuan & Martin 1981). Ferguson (1989b) identifies a total of 35 candidate BCDs in the FCC, but remarks that there are very few BCDs in the Fornax Cluster (only five of the candidates are classified as probable cluster members).

Our spectroscopy of 19 of the candidate BCDs has found that nearly all of these are background galaxies, with only three actually in the cluster – FCC 32, FCC 33 and FCC 35. All three have detectable Hα emission, so their BCD classification is confirmed. Note that FCC 33 is actually too bright to fall in our dwarf sample. Interestingly, all three of these are in fact members of the spiral-rich 'Fornax SW' subcluster identified in Paper III, and not the main cluster.

The morphological properties of the FCC-classified BCDs are compared to the other Fornax dwarf galaxies in Fig. 11(a) which plots central surface brightness against scalelength. All three BCDs have relatively high surface brightness (compared to the other FCC dwarfs) and high Hα equivalent widths, consistent with a high rate of star formation. However, when we include the new cluster members and spectral classifications in our comparison (Fig. 11b), the FCC-classified BCDs are not so distinctive as a class; there are several other star-forming dwarfs with higher surface brightness, although FCC 35 still stands out because of its exceptionally high Hα equivalent width. There is a significant variation of Hα widths with scalelengths: the mean equivalent width is 37 Å for dwarfs with scalelengths less than 4.5 arcsec, compared to 10 Å for larger dwarfs; the distributions differ at a KS significance of 92 per cent. This suggests that the star forming region is very compact.
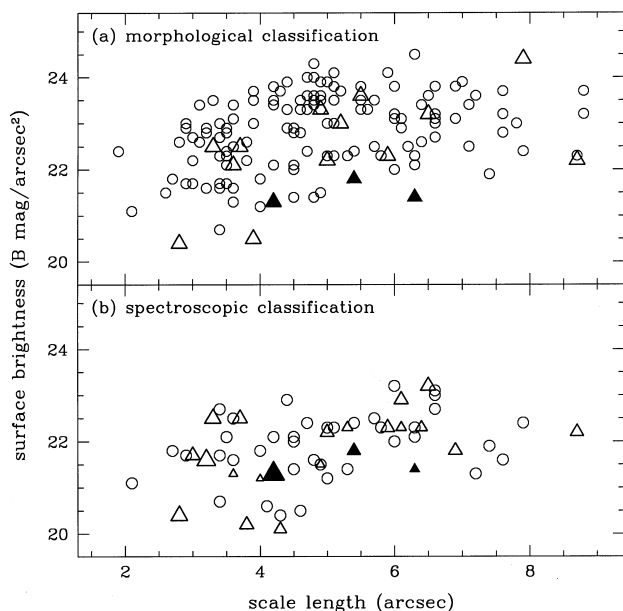
Figure 11. Diagram of surface brightness against scalelength for dwarf cluster members ($b_J > 15.0$). The classifications are shown as early types (circles) and late types (triangles). (a) All probable dwarf cluster members from the FCC using morphological classification; the three BCDs are shown as filled triangles. (b) All dwarfs spectroscopically classified from our FLAIR-II observations. The size of the triangles is scaled to the logarithm of the Hα equivalent width.

Apart from FCC 35 we cannot identify the FCC-classified BCDs as a separate class from our measured parameters (scalelength, magnitude, surface brightness or Hα equivalent width) in our FLAIR-II sample. There are other new cluster members that could also be classified as BCDs, especially those in the low scalelength, high surface brightness region of Fig. 11(b). This agrees with the conclusions of Marlowe, Meurer & Heckman (1999) from a study of nearby blue 'amorphous' star-forming dwarf galaxies. They found that blue amorphous galaxies were indistinguishable from blue starburst dwarfs selected by other means such as BCDs and H II galaxies. On the basis of our measurements we can make a stronger statement for the star-forming dwarfs in the Fornax Cluster: there is no evidence for two distinct populations of 'compact' and 'irregular' star-forming dwarfs. Instead we find that their distribution of scale sizes is continuous and is not significantly different to that of the dwarf ellipticals. The use of 'BCD' as a separate class is confusing here, as it implies a dichotomy not seen in our data. We will therefore avoid any morphological sub-classifications of the late-type dwarfs in our discussion of their evolution below; we limit ourselves to a simple classification of the dwarfs into just two classes: early and late-types based on quantitative Hα equivalent width measurements.

5.3 Evolution of dwarf galaxies

In previous studies of dwarf galaxies in the Virgo cluster (Drinkwater & Hardy 1991; Drinkwater et al. 1996), possible evolutionary relationships between BCDs, dwarf elliptical and dwarf irregular galaxies were examined. It was concluded that there were very few, if any, star-forming dwarfs in Virgo of intermediate size between the BCDs and dwarf irregulars, and in consequence that there was no existing population of star-forming galaxies that could be progenitors of the dE cluster population (see

also Bothun et al. 1986) However, in the Virgo analysis (Drinkwater et al. 1996), the sample was only complete for very compact galaxies and relied on morphological classifications for the intermediate-sized dwarfs. Our current sample of Fornax Cluster dwarfs includes the full range of scale sizes and, in consequence, requires us to revise the conclusions of Drinkwater et al. (1996).

To see the effects of our improved sample we compare Fig. 11(b) with the earlier plot of Drinkwater & Hardy (1991, fig. 4) based on charge-coupled device (CCD) measurements of individual Virgo dwarfs. From the Virgo sample it was concluded that the star-forming dwarfs – BCDs and irregulars, as defined by morphological classifications – occupied two extreme regions of the diagram at small and large scales respectively, with no late-type dwarfs at intermediate scales. In our new data the region of the diagram previously only occupied by dEs of intermediate scale sizes (5–10 arcsec) is also populated with star-forming dwarfs: galaxies with the whole range of scalelengths measured have detected emission lines. On the basis of this diagram alone we can now revise the conclusion of Drinkwater et al. (1996) that there is no current population of star-forming progenitors of cluster dwarf ellipticals. As we now find star-forming dwarfs at all scalelengths, it is much more plausible to model dwarf galaxy evolution by transformations from late- to early-type dwarfs. To determine the factors that drive the evolution we must however examine the distribution of galaxies within the cluster.

The projected distribution of all Fornax galaxies in Fig. 8 suggests immediately that the star-formation activity in the cluster is not concentrated in the same regions as the early-type galaxies. The late-type galaxies are plotted as symbols with sizes related to their absolute star formation rates. These were calculated using a relation derived from Kennicutt (1992): $2.7 \times 10^{-12}(L_B/L_{B\odot})EW$ (Hα) $M_\odot\,y^{-1}$. The figure shows the large amount of star formation taking place in the SW subcluster, $3\,M_\odot\,y^{-1}$ out of a total of $11\,M_\odot\,y^{-1}$ for the whole cluster. The giant galaxies are included in this total star formation rate, so it is entirely dominated by NGC 1365 (nearer the cluster centre) producing $6\,M_\odot\,y^{-1}$.

If we concentrate instead on the dwarf galaxies alone and ignore the spiral-rich SW subcluster, the radial distributions in Fig. 9(c) confirm the deficit of star-forming dwarfs at small projected radii from the centre of the cluster. The fraction of late-type dwarfs falls from 44 per cent at radii greater than 105 arcmin to 25 per cent at smaller radii (the radial distributions differ at a KS confidence level of 85 per cent). This is consistent with the normal density–morphology relation seen for more luminous cluster galaxies. The five star-forming dwarfs found at small projected radius from the centre have lower surface brightness and star formation rates than the other star-forming dwarfs, but the difference is not statistically significant because of the small sample. Our data are therefore consistent with the cluster core being entirely devoid of star-forming dwarfs, the five 'central' dwarfs being physically located in front of or behind the core. The lack of any star-forming dwarfs in the cluster centre provides strong evidence against a very simple evolutionary model in which all dwarfs undergo short, sporadic bursts of star formation (e.g. Davies & Phillipps 1988). A number of processes have been proposed to explain the density–morphology relation, mainly in the context of the giant galaxy population of clusters. There is strong evidence from radio observations that ram pressure stripping can remove the gas from spirals that pass near the cluster cores (van Gorkom 1996), although it has been argued that this is not such an important process for the dwarf galaxy population of poor clusters like Virgo
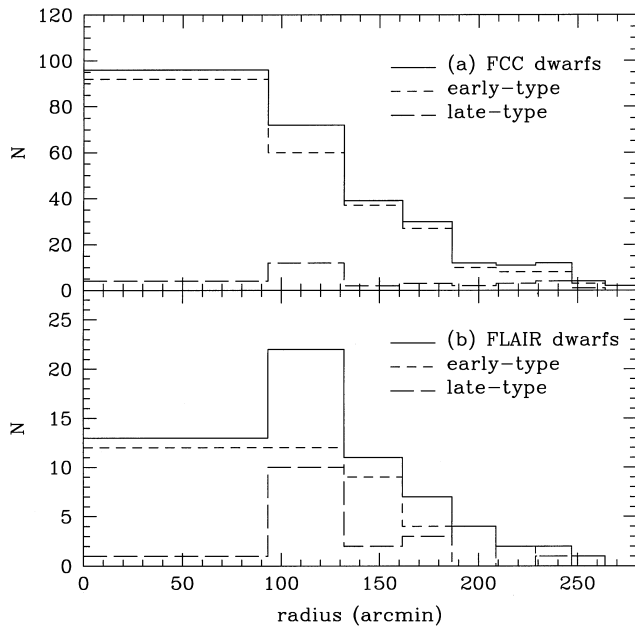
Figure 12. Radial distribution of dwarf galaxies in the Fornax Cluster. The plots give the number of galaxies in annuli of equal area, so the numbers in each bin are directly comparable. In (a), the dwarfs are separated by their FCC morphological classifications (248 early-type and 31 late-type dwarfs). In (b), the dwarfs are separated by their spectral classifications from our FLAIR data (40 early-type and 22 late-type dwarfs). The excess of late-type dwarfs at radii between 100 and 130 arcmin is evident in both plots.

and Fornax (Ferguson & Binggeli 1994) because of the lower central gas density. More recently there has been considerable discussion of dynamical evolution whereby tidal forces from either the cluster or the larger member galaxies can result in significant morphological evolution, enough to convert dwarf irregulars to dwarf ellipticals (Moore, Lake & Katz 1998; Mayer et al. 2001). The second process ('tidal stirring') was proposed in the context of galaxies in the Local Group rather than a rich cluster, but it may also apply in a poor cluster such as Fornax, whose central mass is not much greater than that of the local group.

The *cumulative* radial distribution of late-type dwarfs in Fig. 9(c) exhibits a sharp jump between projected radii of 100 and 120 arcmin. This corresponds to an increased density at that particular radius as is shown in Fig. 12 which plots the surface density of the dwarfs as a function of projected radius. There is a large increase in the number of late-type dwarfs at projected physical radii around 600 kpc, which is evident in the FCC data as well as our smaller FLAIR sample. This concentration resembles that of post starburst galaxies at similar radii around rich clusters reported by Dressler et al. (1999). Some process such as interaction (e.g. Moss & Whittle 1993) is triggering star formation as the dwarfs reach this particular radius. The Fornax dwarfs show significant evidence of current infall compared to the virialised giant cluster galaxies (see Paper III).

Assuming there is no significant gas stripping at this large distance from the cluster centre, we can estimate the timescale for the current star formation in some of these dwarfs for which H I measurements are available (Schröder, Drinkwater & Richter 2001). Using their H I masses, we can estimate the depletion time-scales assuming the current rates of star formation estimated from the Hα data and an extra factor of order 2 to allow for recycling of

the gas (Kennicutt, Tamblyn & Congdon 1994). The depletion time-scales are 5×10^9 (FCC 35), 3×10^{10} (FCC 113), 1×10^{10} (FCC 139), 5×10^{11} (FCC 302) and 2×10^{10} yr (FCC 306). (The time-scales for the giant star-forming galaxies span a similar range.) Apart from FCC 35 (a special case as it is in the active subcluster), these timescales are all long, of order both the Hubble time and the orbital period of the cluster at this radius (3×10^{10} yr). If the early-type galaxies already in the cluster core once had similar properties, then some active process must have removed the gas as they fell into the cluster; these star formation rates are not high enough to exhaust the gas in a Hubble time.

The dwarf galaxies in Fornax appear to trace a complex evolutionary path. In the cluster core there is virtually no current star formation, although Held & Mould (1994) showed that several of the nucleated dwarf ellipticals have experienced recent star formation activity. This is the classical density–morphology relation seen here for dwarf galaxies, driven by gas removal and morphological transformation. In the outer regions of the cluster however, at a radius of about 600 kpc, there is a concentration of star-forming dwarfs. This resembles a similar concentration of post starburst galaxies at similar radii around rich clusters (Dressler et al. 1999). We plan to obtain blue spectra of the Fornax dwarfs in order to look for post-starburst galaxies. This combination of enhanced star formation in the cluster fringes and complete suppression in the cluster core is very consistent with the results of Hashimoto et al. (1998) who measured the spectral properties of a very large sample of galaxies from the Las Campanas Redshift Survey to determine how star formation rate depends on the local galaxy density. They found that starburst activity was enhanced in regions of intermediate density, but that star formation was suppressed in regions of high density like the centres of galaxy clusters.

6 COMPACT DWARF ELLIPTICAL (M 32-LIKE) CANDIDATES

We observed 97 of the M 32-like cdE candidates listed in the FCC (Tables 3 and 13) and successfully determined redshifts for 76 of these. Only one of these was a cluster member (FCC B2144), but it had a blue spectrum with emission lines, and therefore is a BCD-like galaxy, not a normal red dwarf elliptical (details in Paper I). The remaining 75 cdE candidates found to be background objects are indicated in Table A1.

The FCC criteria for cdE candidates included possible background galaxies, although it was noted that most of these were probably isolated background ellipticals. We calculated absolute magnitudes and estimated scalelengths and surface brightnesses for all 75 cdE candidates in the background sample using a Hubble constant of 75 km s^{-1} Mpc^{-1}. These are shown in Fig. 13 along with all the other galaxies we measured for comparison. Most of the cdE candidates have redshifts of 10 000 km s^{-1} or more and absolute magnitudes brighter than $M_B = -18$ and are giant ellipticals as suggested. Two of the candidate cdEs were somewhat closer: FCCB 278 at $v = 7960$ km s^{-1}, $M_B = -17.5$ and FCCB 712 at $v = 6670$ km s^{-1}, $M_B = -17.2$ with scalelengths of 1000 and 780 pc respectively. These are both much more luminous and larger than M 32 which has an absolute magnitude $M_B = -15.8$ (Mateo 1998) and scalelength of 80 pc (see below). We therefore conclude that none of the candidate cdEs listed in the FCC resemble M 32 (see locations of filled symbols in Fig. 13).
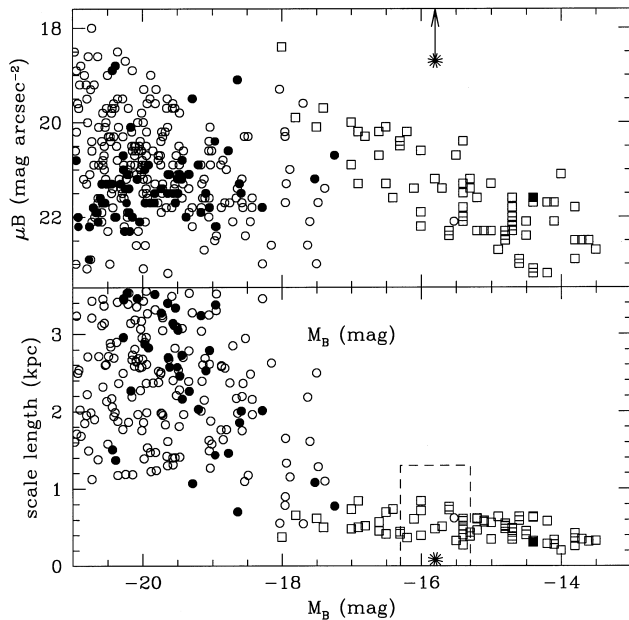
Figure 13. Structural parameters of candidate cdE (M 32-like) galaxies with measured redshifts as a function of absolute magnitude. In each plot, background galaxies are plotted as circles and cluster members as squares; the candidate cdE galaxies (as listed in the FCC) are plotted as filled symbols. Upper panel: the distribution of central surface brightness with the position of M 32 given by a mean surface brightness which is a lower limit to the central surface brightness (see text). Lower panel: the distribution of physical scalelengths. The position M 32 would occupy is indicated by the large asterisk and the region of M 32-like objects discussed in the text is enclosed by dashed lines. Note that these structural parameters were calculated from exponential fits to the photographic images and have not been corrected for seeing or cosmological fading.

Following the philosophy of this paper of replacing morphological classifications by quantitative measures, we have included in Fig. 13 the parameters of all the compact-appearing galaxies we measured in addition to the cdE candidates. We also indicate the position that M 32 would occupy in the diagram, although the values of its surface brightness and scalelength parameters are not directly comparable as they are based on images of much higher physical resolution than our data. We use the data of Faber et al. (1989) who measure an effective radius of 140 pc (corresponding to an exponential scalelength of 80 pc) and a mean surface brightness within this radius of $\mu B = 18.7$ mag arcsec^{-2} which gives a lower limit for the central surface brightness.

As discussed above, none of the cdE candidates have sizes and luminosities comparable to M 32, but there are a number of compact cluster galaxies in our sample with similar luminosities as indicated by the dashed line in the figure. There are 20 galaxies in this region; nine (including the only background galaxy FCCB 138) have late-type spectroscopic classifications, but the rest are early-type dwarf galaxies (most with FCC classifications of dE,N). These are potentially similar to M 32, but their much larger scalelengths, according to Fig. 13, show that they are not like M 32, as we might expect as they were not classified as cdE candidates in the FCC.

As a result of our investigation of 75 cdE candidates from the FCC and our own, larger, sample of compact galaxies, we conclude that there are no galaxies like M 32 in the Fornax cluster. A similar search for M 32-like galaxies in the Leo group was unsuccessful (Ziegler & Bender 1998), so this may be a general result. These

observations give some support to the conclusions of Nieto & Prugniel (1987) that tidal stripping is not a realistic formation scenario for such objects. However, we do note that tidal stripping does appear to be a realistic explanation (Bekki, Couch & Drinkwater 2001) for the formation of a less luminous class of compact galaxy recently found in the Fornax Cluster (Drinkwater et al. 2000a)

7 CONCLUSIONS

In this paper we have made the first detailed study of the Fornax Cluster in which morphological and membership classifications have been replaced by quantitative image parameters and spectroscopic memberships. The image parameters were obtained from complete catalogues of digitized sky survey plates, allowing for a statistical approach to our analysis. The spectroscopic data have allowed us to confirm the membership of many cluster galaxies originally estimated from visual morphological classification (Ferguson 1989b). In our search for compact cluster galaxies we have found nine new compact cluster dwarf galaxies previously classified as background galaxies.

We used our spectroscopic data to estimate star formation rates from Hα emission equivalent widths. The total star formation rate for the cluster is dominated by the giant spiral NGC 1365, but the remaining star formation is concentrated in a separate subcluster we have identified 3° south-west of the main cluster, centred on NGC 1316 (Fornax A) as described in Paper III. Among the dwarf galaxies we find a much higher incidence of detected star formation than was suggested by the original morphological classifications. Of the 62 dwarf galaxies we measured, 35 per cent are star-forming but only 19 per cent were classified as late types. Our spectral classification is based on emission from the cores of each galaxy, but we estimate that a correction to include the whole galaxy would change at most one of our classifications.

Only three of the BCD candidates were found to be cluster members. Our data do not support the existence of a well-defined separate class of BCD-like objects, but rather we detect actively star forming dwarf galaxies over the whole range of measured sizes. We have also shown that there is no group of very compact BCDs without corresponding early-type dwarfs at the same scale sizes. The distribution of scale sizes is consistent with model of dwarf galaxy evolution involving morphological transformation from late- to early-type galaxies. This is in contrast to earlier work on Virgo Cluster dwarfs (Drinkwater et al. 1996) which was not based on spectroscopic classifications.

The fraction of star-forming dwarf galaxies in Fornax drops significantly towards the cluster centre. This observation alone is sufficient to rule out simple evolutionary models where the dwarfs form a single population with each dwarf experiencing regular short bursts of star formation. We estimate long gas depletion timescales for the few dwarfs with detected H I emission. This implies that an active process of gas depletion is needed to transform them to quiescent galaxies like the central dwarfs. We conclude that star formation in dwarf cluster galaxies is a complex process influenced by their environment: there are less star-forming dwarfs at the cluster centre presumably due to some form of gas stripping. High rates of star formation are found at the edges of the cluster, perhaps stimulated by tidal interactions.

Our data also allowed us to look at the candidate compact elliptical galaxies listed by Ferguson (1989b). We find that none of these have properties like M 32: they are all background giant ellipticals except for one cluster member which is less luminous

than M 32 and is also a spectroscopic late-type galaxy. We broadened our search to the larger sample of compact galaxies that we observed and found that, although some of the brighter cluster dwarfs had similar luminosities to M 32, none of them had similarly small scalelengths. We therefore confirm our earlier conclusions (Drinkwater & Gregg 1998) that there are no galaxies like M 32 in the Fornax Cluster. We do note however that our 2dF observations have revealed a population of very compact objects at the centre of the cluster which resemble low-luminosity ($-13 <$ $M_B < -11$) versions of M 32 (Drinkwater et al. 2000a).

ACKNOWLEDGMENTS

REFERENCES

Bekki K., Couch W. J., Drinkwater M. J., 2001, ApJ, 552, L105

Binggeli B., Popescu C. C., Tammann G. A., 1993, A&AS, 98, 275

Binggeli B., Sandage A., Tammann G. A., 1985, AJ, 90, 1681

Binggeli B., Sandage A., Tarenghi M., 1984, AJ, 89, 64

Bothun G. D., Mould J. R., Caldwell N., MacGillivray H. T., 1986, AJ, 92, 1007

Bureau M., Mould J. R., Staveley-Smith L., 1996, ApJ, 463, 60

Colless M., Dunn A. M., 1996, ApJ, 458, 435

Couch W. J., Ellis R. S., MacLaren I., Malin D. F., 1991, MNRAS, 249, 606

Davies J. I., Phillipps S., 1988, MNRAS, 233, 553

Davies J. I., Phillipps S., Cawson M. G. M., Disney M. J., Kibblewhite E. J., 1988, MNRAS, 232, 239

de Vaucouleurs G., de Vaucouleurs A., Corwin J. R., Buta R. J., Paturel G., Fouque P., 1991, Third reference catalogue of Bright galaxies. Springer-Verlag, New York, p. 15

Diaferio A., 1999, MNRAS, 309, 610

Dressler A., Smail I., Poggianti B. M., Butcher H., Couch W. J., Ellis R. S., Oemler A. J., 1999, ApJS, 122, 51

Drinkwater M. J., Gregg M. D., 1998, MNRAS, 296, L15 (Paper I)

Drinkwater M., Hardy E., 1991, AJ, 101, 94

Drinkwater M. J., Currie M. J., Young C. K., Hardy E., Yearsley J. M., 1996, MNRAS, 279, 595

Drinkwater M. J., Gregg M. D., Holman B. A., 1997, in Arnaboldi M., Da Costa G. S., Saha P., eds, ASP Conf. Ser. Vol. 116, The Nature of Elliptical Galaxies; 2nd Stromlo Symposium. Astron. Soc. Pac., San Francisco, p. 287

Drinkwater M. J., Jones J. B., Gregg M. D., Phillipps S., 2000a, Pub. Ast. S. Aust., 17, 227

Drinkwater M. J. et al., 2000b, A&A, 355, 900

Drinkwater M. J., Gregg M. D., Colless M., 2001, ApJ, 548, L139

Faber S. M., 1973, ApJ, 179, 423

Faber S. M., Wegner G., Burstein D., Davies R. L., Dressler A., Lynden-Bell D., Terlevich R. J., 1989, ApJS, 69, 763

Ferguson H. C., 1989a, Ap&SS, 157, 227

Ferguson H. C., 1989b, AJ, 98, 367

Ferguson H. C., Binggeli B., 1994, A&AR, 6, 67

Ferguson H. C., Sandage A., 1988, AJ, 96, 1520

Gallagher J. S., Hunter D. A., 1989, AJ, 98, 806

Hashimoto Y., Oemler A. J., Lin H., Tucker D. L., 1998, ApJ, 499, 589

Held E. V., Mould J. R., 1994, AJ, 107, 1307

Hilker M., Infante L., Vieira G., Kissler-Patig M., Richtler T., 1999, A&AS, 134, 75

Holman B., Drinkwater M., Gregg M., 1995, in Chapman J., Cannon R., Harrison S., Hidayat B., eds, ASP Conf. Ser. Vol. 84, IAU Colloq. 148, The Future Utilisation of Schmidt Telescopes. Astron. Soc. Pac., San Francisco, p. 107

Irwin M., Maddox S., McMahon R., 1994, Spectrum, 2, 14

Irwin M. J., Davies J. I., Disney M. J., Phillipps S., 1990, MNRAS, 245, 289

Kennicutt R. C., 1992, ApJ, 388, 310

Kennicutt R. C., Tamblyn P., Congdon C. E., 1994, ApJ, 435, 22

Kurtz M. J., Mink D. J., 1998, PASP, 110, 934

Loveday J., 1996, MNRAS, 278, 1025

Loveday J., Peterson B. A., Maddox S. J., Efstathiou G., 1996, ApJs, 107, 201

Maddox S. J., Efstathiou G., Sutherland W. J., Loveday J., 1990, MNRAS, 243, 692

Marlowe A. T., Meurer G. R., Heckman T. M., 1999, ApJ, 522, 183

Mateo M. L., 1998, ARA&A, 36, 435

Mayer L., Governato F., Colpi M., Moore B., Quinn T., Wadsley J., Stadel J., Lake G., 2001, ApJL, 547, L123

Michard R., Nieto J.-L., 1991, A&A, 243, L17

Moore B., Lake G., Katz N., 1998, ApJ, 495, 139

Morshidi-Esslinger Z., Davies J. I., Smith R. M., 1999, MNRAS, 304, 297

Moss C., Whittle M., 1993, ApJ, 407, L17

Mould J. R. et al., 2000, ApJ, 528, 655

Nieto J.-L., Prugniel P., 1987, A&A, 186, 30

Parker Q. A., Watson F. G., 1995a, FLAIR System Users Guide, AAO User Manual 31.1. Anglo-Australian Observatory, Sydney

Parker Q. A., Watson F. G., 1995b, Proc. SPIE, 2476, 34

Press W. H., Teukolsky S. A., Vetterling W. T., Flannery B. P., 1992, Numerical recipes in C: the art of scientific computing. 2nd edn. Cambridge Univ. Press, Cambridge

Royston J. P., 1982, Appl. Stat., 31, 176

Schröder A., Drinkwater M. J., Richter O.-G., 2001, A&A, in press

Thuan T. X., Martin G. E., 1981, ApJ, 247, 823

Tody D., 1993, in Hanisch R. J., Brissenden R. J. V., Barnes J., eds, ASP. Conf. Ser. Vol. 52, Astronomical Data Analysis Software and Systems II. Astron. Soc. Pac., San Francisco, p. 173

van Gorkom J., 1996, in Skillman E. D., ed., ASP Conf. Ser. Vol. 106, The Minnesota Lectures on Extragalactic Neutral Hydrogen. Astron. Soc. Pac., San Francisco, p. 293

Ziegler B. L., Bender R., 1998, A&A, 330, 819

APPENDIX A: BACKGROUND GALAXIES

The majority of the galaxies that we measured were background objects behind the Fornax Cluster as expected from our compact

Table A1. Catalogue of all background galaxies with measured redshifts.

FCC	RA (J2000) Dec	cz	σ_{cz}	cdE	FCC	RA (J2000) Dec	cz	σ_{cz}	cdE
FCCB 0102	03:22:26.6 −36:15:30	25572	99		FCCB 0599	03:29:23.6 −37:21:28	12069	27	
FCCB 0116	03:22:42.7 −36:26:26	19364	59		FCCB 0598	03:29:25.9 −35:08:29	13926	38	*
FCCB 0119	03:22:46.6 −36:21:12	19231	43		FCCB 0600	03:29:28.1 −34:29:12	31614	73	
FCCB 0126	03:22:52.9 −36:46:03	12131	45		FCCB 0605	03:29:31.0 −37:28:31	19126	43	
FCCB 0127	03:22:57.8 −34:17:16	15727	21		FCCB 0616	03:29:47.9 −36:46:57	29276	77	
FCCB 0138	03:23:02.4 −36:54:09	4184	34		FCCB 0624	03:29:55.4 −34:39:33	28591	97	
FCCB 0153	03:23:19.0 −36:00:22	19729	85		FCCB 0631	03:30:01.4 −35:36:26	16719	20	
FCCB 0162	03:23:23.7 −37:32:10	12113	46		FCCB 0638	03:30:08.2 −38:08:58	29280	93	
FCC 24	03:23:31.7 −34:36:34	13222	14		FCCB 0634	03:30:10.7 −34:14:59	16333	67	*
FCCB 0185	03:23:37.6 −36:05:50	19296	55		FCCB 0653	03:30:24.5 −36:22:35	19206	41	
FCCB 0183	03:23:38.2 −35:06:53	26186	44		FCCB 0650	03:30:25.3 −33:38:53	36348	102	
FCCB 0178	03:23:38.2 −33:27:42	20402	36		FCCB 0651	03:30:25.7 −33:58:58	36699	52	
FCCB 0187	03:23:38.2 −36:53:14	12315	51		FCCB 0654	03:30:27.3 −34:40:15	19017	32	
FCCB 0192	03:23:39.6 −36:54:31	19608	41		FCCB 0657	03:30:30.5 −35:22:08	13335	22	
FCCB 0208	03:23:51.3 −35:05:34	26163	65		FCCB 0674	03:30:41.9 −36:55:16	14002	21	
FCCB 0206	03:23:52.1 −34:05:14	19553	86		FCCB 0672	03:30:44.4 −34:38:45	28736	99	
FCCB 0213	03:23:56.4 −34:54:29	19408	61		FCCB 0679	03:30:45.0 −38:11:24	12321	43	
FCCB 0216	03:23:58.7 −34:19:40	19229	88		FCCB 0676	03:30:49.7 −34:38:44	28444	35	
FCCB 0219	03:23:59.5 −36:03:57	19350	33		FCCB 0693	03:30:57.7 −37:19:01	18018	56	
FCCB 0248	03:24:24.0 −37:20:32	24905	99	*	FCCB 0692	03:31:00.1 −35:28:09	18974	76	*
FCCB 0245	03:24:25.6 −34:22:26	19371	42		FCCB 0691	03:31:01.2 −34:23:28	21139	61	
FCCB 0249	03:24:26.5 −36:35:27	17043	37		FCCB 0702	03:31:04.6 −37:55:29	17661	24	
FCCB 0255	03:24:36.6 −34:06:14	15265	101		FCCB 0703	03:31:08.6 −37:07:09	34247	45	
FCCB 0252	03:24:36.8 −32:34:13	19156	58		FCCB 0707	03:31:12.6 −36:14:26	6543	53	
FCCB 0258	03:24:39.3 −35:33:53	29831	39		FCCB 0712	03:31:19.6 −35:35:01	6666	47	*
FCCB 0265	03:24:44.8 −36:42:48	28839	78		FCCB 0718	03:31:26.3 −35:05:07	21130	33	
FCCB 0266	03:24:45.5 −36:19:42	19634	62		FCCB 0727	03:31:30.3 −37:42:04	23734	45	
FCCB 0272	03:24:48.0 −36:18:14	19421	42		FCCB 0740	03:31:40.6 −37:21:57	50131	91	
FCCB 0274	03:24:52.0 −37:04:32	22077	42		FCCB 0734	03:31:41.5 −34:17:03	24942	56	
FCCB 0276	03:24:56.4 −34:39:17	32670	99	*	FCCB 0731	03:31:41.8 −32:34:03	22336	80	*
FCCB 0278	03:24:58.0 −34:47:17	7957	38	*	FCCB 0743	03:31:48.2 −34:23:45	15838	39	
FCCB 0288	03:25:12.1 −33:05:02	19875	66		FCCB 0747	03:31:49.5 −37:04:10	18290	27	
FCCB 0290	03:25:16.4 −32:28:14	19095	74		FCCB 0753	03:31:51.8 −38:14:52	12129	64	
FCCB 0305	03:25:23.5 −37:15:55	16334	37		Name 2	03:31:54.9 −34:30:45	21972	33	
FCCB 0298	03:25:23.5 −33:03:25	19675	62	*	FCCB 0754	03:31:55.6 −36:21:07	29967	35	
FCCB 0309	03:25:30.5 −34:52:08	15359	54	*	FCCB 0757	03:31:59.5 −35:24:34	20979	23	
FCCB 0311	03:25:34.3 −33:52:21	14306	41		FCCB 0761	03:31:59.5 −36:25:17	30043	71	*
FCCB 0315	03:25:38.9 −32:01:07	13763	30	*	FCCB 0774	03:32:04.1 −37:59:58	20140	59	
FCCB 0331	03:25:43.3 −37:31:26	16664	39	*	FCCB 0777	03:32:08.2 −37:47:21	24327	43	
FCCB 0332	03:25:45.0 −37:35:60	24721	64		FCCB 0786	03:32:17.0 −37:22:42	19194	46	*
FCCB 0328	03:25:46.8 −33:58:56	34526	63		FCCB 0792	03:32:24.1 −37:48:14	24476	51	
FCCB 0339	03:25:53.4 −35:40:14	15902	50		FCCB 0793	03:32:24.9 −38:05:47	17712	67	
FCCB 0336	03:25:53.6 −33:43:37	19490	73		FCCB 0797	03:32:34.1 −33:18:19	27130	78	*
FCCB 0337	03:25:53.6 −34:19:52	15251	44		FCCB 0801	03:32:35.9 −36:33:10	11986	22	
FCCB 0346	03:25:59.0 −36:01:43	19421	58	*	FCCB 0805	03:32:49.4 −32:40:07	19756	111	
FCCB 0347	03:26:02.2 −34:06:35	19506	29		FCCB 0817	03:32:51.1 −34:51:07	21467	60	
FCCB 0358	03:26:08.2 −37:43:10	24981	69		FCCB 0816	03:32:51.5 −34:29:30	14374	42	*
FCCB 0359	03:26:13.0 −34:48:40	15655	78		FCCB 0815	03:32:53.3 −33:08:22	38232	37	*
FCCB 0362	03:26:16.8 −33:33:02	20554	74		FCCB 0829	03:33:00.6 −35:27:07	14369	47	
FCCB 0373	03:26:17.1 −37:54:14	19297	80		FCCB 0838	03:33:04.4 −37:07:13	23859	22	
FCCB 0379	03:26:20.3 −36:48:05	19222	37		FCCB 0847	03:33:13.4 −35:04:29	21510	35	*
FCCB 0378	03:26:22.7 −35:02:28	15650	83	*	FCCB 0854	03:33:14.1 −36:34:02	30148	37	
FCCB 0376	03:26:23.5 −34:05:03	19686	102	*	FCCB 0858	03:33:19.3 −35:20:43	21157	35	
FCCB 0389	03:26:29.5 −36:10:19	31840	44		FCCB 0859	03:33:19.6 −35:40:32	19122	58	
FCCB 0388	03:26:33.0 −32:40:05	22219	66		FCCB 0860	03:33:24.7 −32:38:24	22145	58	*
FCCB 0391	03:26:35.1 −33:30:21	14783	42		FCCB 0871	03:33:36.2 −35:10:03	21396	93	*
FCCB 0403	03:26:41.7 −34:59:35	27896	51	*	FCCB 0874	03:33:40.6 −33:00:54	26930	105	*
FCCB 0413	03:26:48.7 −34:15:12	26202	105		FCCB 0883	03:33:41.4 −38:21:52	20210	55	
FCCB 0420	03:26:51.5 −34:22:24	9351	60		FCC 123	03:33:43.4 −35:51:33	15483	60	
FCCB 0422	03:26:51.5 −35:14:37	19731	29		FCCB 0882	03:33:46.9 −34:19:44	21982	57	*
FCCB 0424	03:26:53.2 −34:20:04	14742	33		FCCB 0902	03:33:53.9 −35:51:43	15463	42	
Name 1	03:27:00.2 −35:48:55	25548	44		FCCB 0897	03:33:56.4 −32:39:37	22471	68	
FCCB 0438	03:27:00.3 −36:35:42	13660	34		FCCB 0909	03:34:01.4 −33:55:24	24673	42	
FCCB 0446	03:27:09.2 −37:09:11	19202	64	*	FCCB 0920	03:34:03.3 −37:19:43	23435	64	
FCCB 0443	03:27:09.3 −34:47:41	13538	51		FCCB 0916	03:34:06.5 −33:54:32	27963	81	
FCCB 0447	03:27:09.4 −38:19:05	9287	65		FCCB 0921	03:34:07.5 −34:32:23	21186	61	
FCCB 0448	03:27:11.5 −37:27:52	17520	45	*	FCCB 0926	03:34:09.3 −34:05:54	19833	54	*
FCCB 0441	03:27:11.5 −32:42:16	16671	34		FCCB 0925	03:34:10.0 −33:39:14	28322	53	
FCCB 0445	03:27:12.9 −33:24:10	19001	71	*	FCCB 0931	03:34:11.5 −37:48:50	19136	39	
FCCB 0453	03:27:16.7 −36:51:57	19167	60		FCCB 0939	03:34:21.7 −35:45:09	21452	35	
FCCB 0450	03:27:18.0 −34:41:47	32180	65		FCCB 0938	03:34:24.8 −33:04:30	13972	81	

Table A1 – *continued*

FCC	RA (J2000) Dec	cz	σ_{cz}	cdE	FCC	RA (J2000) Dec	cz	σ_{cz}	cdE
FCCB 0454	03:27:22.6 −33:56:40	9392	45		FCCB 0943	03:34:26.0 −36:49:09	18958	50	
FCCB 0459	03:27:25.2 −35:59:49	6640	32		FCCB 0946	03:34:28.3 −36:53:26	23740	123	
FCCB 0458	03:27:26.8 −33:40:32	39044	102	*	FCCB 0950	03:34:31.6 −36:52:20	18946	79	
FCCB 0466	03:27:30.8 −36:35:02	33769	106		FCCB 0948	03:34:32.5 −35:03:55	19618	21	
FCCB 0469	03:27:30.9 −37:36:28	9253	39		FCCB 0951	03:34:37.7 −35:33:30	28887	63	*
FCCB 0465	03:27:35.0 −33:03:58	34898	96	*	FCCB 0962	03:34:46.0 −36:21:51	20894	58	*
FCCB 0477	03:27:36.5 −37:27:23	18887	24		FCCB 0963	03:34:48.0 −35:33:31	19118	68	*
FCCB 0475	03:27:37.7 −33:48:24	14121	190	*	FCCB 0960	03:34:49.2 −33:13:22	30514	89	
FCCB 0471	03:27:38.0 −32:46:02	20428	62		FCCB 0968	03:34:50.8 −36:02:03	19213	40	
FCCB 0482	03:27:43.7 −35:01:49	15508	86	*	FCCB 0986	03:35:05.9 −35:51:31	39410	95	*
FCCB 0490	03:27:45.5 −37:36:15	9331	32		FCCB 0994	03:35:06.0 −37:54:51	19073	64	
FCCB 0501	03:27:57.9 −36:03:53	24336	88		FCCB 0981	03:35:06.0 −33:38:12	15970	77	
FCCB 0502	03:27:58.3 −35:56:34	24294	90		FCCB 0984	03:35:08.6 −32:16:16	13908	40	
FCCB 0513	03:28:08.0 −35:02:44	31301	51		FCCB 0993	03:35:13.3 −32:25:26	13726	25	
FCCB 0516	03:28:13.4 −34:12:35	19550	39		FCCB 1009	03:35:17.6 −36:15:07	20881	41	
FCCB 0517	03:28:14.4 −34:38:37	14735	68	*	FCCB 1004	03:35:19.4 −33:06:42	30604	99	
FCCB 0522	03:28:15.6 −36:03:46	30321	52		FCCB 1014	03:35:19.5 −36:22:38	18888	52	
FCCB 0532	03:28:24.3 −34:52:25	15107	28		FCCB 1013	03:35:20.0 −35:59:30	15564	61	*
FCCB 0535	03:28:27.6 −34:55:45	15401	79		FCCB 1020	03:35:29.6 −33:13:55	29463	139	
FCCB 0542	03:28:38.4 −32:49:37	19235	62		FCCB 1027	03:35:34.4 −36:18:54	12111	104	
FCCB 0548	03:28:43.4 −33:59:52	20549	40		FCCB 1029	03:35:39.4 −36:17:48	14341	48	
FCCB 0547	03:28:44.3 −32:44:54	19238	34		FCCB 1034	03:35:47.5 −32:58:42	38808	60	*
FCCB 0556	03:28:46.5 −37:13:34	19310	42		FCCB 1056	03:36:07.1 −33:24:02	22243	30	
FCCB 0561	03:28:54.0 −36:34:47	19276	65		FCCB 1081	03:36:22.3 −38:10:19	19068	61	
FCCB 0567	03:28:56.5 −38:04:18	19855	52		FCCB 1083	03:36:25.1 −36:53:30	18824	45	
FCCB 0566	03:28:56.7 −36:05:05	19156	39		FCCB 1087	03:36:27.5 −37:15:43	21315	106	
FCCB 0570	03:28:57.5 −37:42:46	17456	73	*	FCCB 1090	03:36:27.7 −37:57:25	19234	44	
FCCB 0576	03:29:05.0 −35:19:34	15943	76		FCCB 1079	03:36:27.9 −33:58:28	21953	96	
FCCB 0582	03:29:10.0 −35:52:35	16759	40		FCCB 1084	03:36:30.2 −33:44:01	36261	105	*
FCCB 0580	03:29:10.2 −34:57:41	15360	46		FCCB 1085	03:36:30.9 −33:27:26	28100	87	
FCCB 0594	03:29:22.3 −37:06:60	30911	107	*	FCCB 1094	03:36:38.3 −34:22:56	17777	48	

Notes: the names of the galaxies not listed in the FCC are given in Table 7. The asterisks indicate cdE candidates from the FCC.
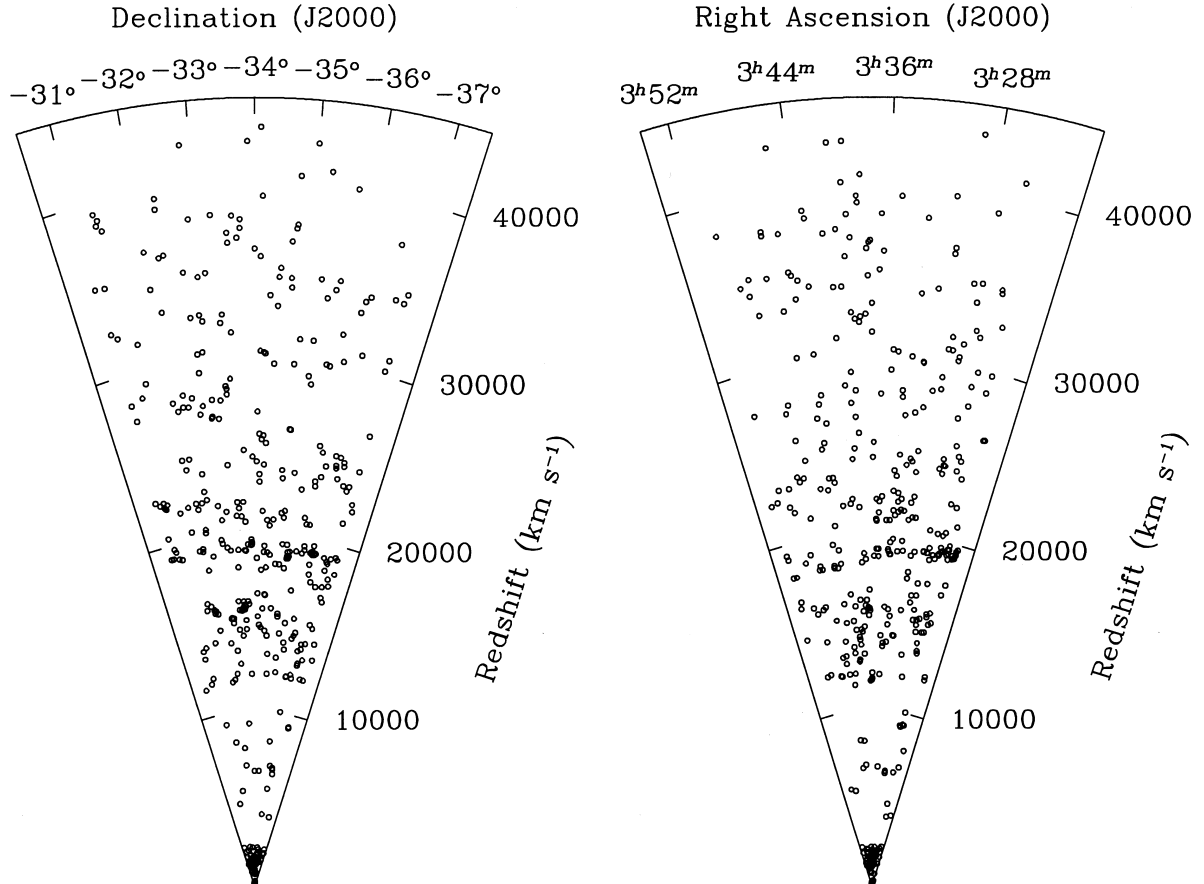

Figure A1. Distribution of the observed galaxies.

Table A2. Catalogue of all background galaxies with measured redshifts (continued).

FCC	RA (J2000) Dec	cz	σ_{cz}	cdE	FCC	RA (J2000) Dec	cz	σ_{cz}	cdE
FCCB 1100	03:36:41.6 −34:59:27	19240	36		FCCB 1611	03:42:43.4 −36:16:08	23108	99	
FCCB 1103	03:36:43.0 −34:45:34	38389	65	*	FCCB 1618	03:42:50.0 −35:07:57	18469	74	
FCCB 1106	03:36:47.6 −34:32:29	19244	37		FCCB 1619	03:42:53.6 −34:11:60	16161	38	
FCCB 1107	03:36:49.7 −33:22:46	28146	51	*	FCCB 1621	03:42:54.1 −34:47:51	19245	71	
FCCB 1109	03:36:53.2 −32:59:20	35175	114	*	FCCB 1632	03:42:54.5 −37:28:30	6411	45	
FCCB 1110	03:36:53.2 −33:33:16	22083	25		FCCB 1626	03:42:54.6 −36:17:56	23392	98	*
FCCB 1116	03:36:54.0 −35:35:52	20941	76		FCCB 1631	03:42:54.6 −37:10:57	15099	23	
FCCB 1134	03:37:08.6 −36:50:10	18833	28		FCCB 1635	03:43:07.1 −32:41:35	38715	77	
FCCB 1143	03:37:17.3 −35:09:26	18909	39		FCCB 1643	03:43:07.9 −34:23:52	38289	48	
FCCB 1144	03:37:19.9 −33:15:20	15765	43		FCCB 1648	03:43:08.3 −37:07:36	26513	57	
FCCB 1147	03:37:22.5 −33:02:29	11702	28	*	FCCB 1654	03:43:16.3 −33:37:54	18228	70	
FCCB 1156	03:37:23.2 −37:35:08	24491	34		FCCB 1660	03:43:21.0 −36:18:18	12150	57	
FCCB 1155	03:37:28.6 −33:02:46	11884	36		FCCB 1663	03:43:23.1 −35:12:24	23378	102	
FCCB 1158	03:37:32.1 −32:26:02	31599	74		FCCB 1668	03:43:29.0 −33:41:04	27643	56	
FCCB 1173	03:37:32.8 −37:53:28	33243	59		FCCB 1666	03:43:29.6 −33:27:01	22718	112	
FCCB 1162	03:37:33.4 −32:21:18	11813	50	*	FCCB 1676	03:43:31.6 −36:39:06	14054	61	
FCCB 1171	03:37:33.5 −36:18:26	25261	69		FCCB 1680	03:43:33.5 −36:18:28	25428	78	
FCCB 1169	03:37:35.3 −34:39:51	37055	56		FCCB 1684	03:43:34.1 −37:17:03	34346	68	*
FCCB 1178	03:37:42.7 −35:19:11	36840	42		FCCB 1681	03:43:35.0 −35:48:02	30490	97	
Name 3	03:37:45.0 −34:48:34	26232	133		FCCB 1686	03:43:39.8 −34:40:06	12759	28	
FCCB 1186	03:37:50.1 −33:11:57	11755	68		FCCB 1682	03:43:40.2 −32:37:25	19578	18	
FCCB 1193	03:37:50.9 −34:29:17	36748	115	*	FCCB 1700	03:43:46.1 −37:37:43	13214	45	
FCCB 1195	03:37:51.4 −35:47:35	33550	63		FCCB 1695	03:43:47.4 −33:54:49	52379	95	*
FCCB 1192	03:37:52.0 −33:36:45	15747	72		FCCB 1707	03:43:57.9 −36:12:20	25083	59	
FCCB 1200	03:37:54.9 −36:43:52	34831	157	*	FCCB 1714	03:44:00.6 −35:35:28	18250	69	
Name 4	03:37:57.1 −37:25:43	16923	31		FCCB 1711	03:44:04.5 −32:41:14	49995	75	
FCCB 1202	03:38:00.6 −33:34:17	15879	51		FCCB 1727	03:44:12.0 −37:07:34	18379	87	
FCCB 1212	03:38:02.1 −35:59:59	36380	42		FCCB 1739	03:44:21.0 −35:31:56	34769	69	
FCCB 1209	03:38:05.9 −32:25:32	35737	123		FCCB 1749	03:44:29.0 −36:56:09	13145	38	
FCCB 1225	03:38:08.1 −36:19:26	15477	89		FCCB 1754	03:44:30.1 −38:16:49	25287	55	
FCCB 1221	03:38:10.3 −33:17:19	32624	58		FCCB 1762	03:44:41.6 −35:41:31	33718	48	
FCCB 1230	03:38:14.0 −32:51:40	32302	64		FCCB 1769	03:44:44.9 −36:38:41	22825	37	
FCCB 1234	03:38:14.3 −33:38:43	15929	19	*	FCCB 1767	03:44:45.7 −34:55:26	35093	88	
FCCB 1238	03:38:15.9 −34:06:55	14480	40		FCCB 1784	03:44:51.5 −38:34:32	6578	38	
FCCB 1244	03:38:16.6 −37:33:33	13743	38		FCCB 1797	03:45:00.6 −37:36:25	15278	37	
FCCB 1240	03:38:18.1 −33:07:15	32595	64		FCCB 1799	03:45:01.8 −38:22:57	14684	38	
FCCB 1257	03:38:28.3 −34:37:49	16343	53		FCCB 1798	03:45:04.9 −35:30:18	35294	81	
FCCB 1263	03:38:31.3 −35:14:18	40600	52		FCCB 1810	03:45:17.4 −32:12:48	12111	73	
FCCB 1273	03:38:36.4 −36:04:14	18655	48		FCCB 1814	03:45:23.2 −35:45:57	30418	63	*
FCCB 1267	03:38:38.4 −31:53:48	13263	80		FCCB 1816	03:45:26.6 −34:15:45	37560	38	*
FCCB 1271	03:38:39.2 −32:54:37	32491	60	*	FCCB 1848	03:45:50.1 −38:08:35	13437	51	
FCCB 1278	03:38:42.8 −34:20:37	16016	33		FCCB 1854	03:45:59.5 −34:34:06	18268	75	
FCCB 1276	03:38:44.3 −32:39:18	39020	57	*	FCCB 1857	03:45:59.9 −35:32:14	33119	55	
FCCB 1279	03:38:45.1 −32:47:54	32170	77		FCC 311	03:46:18.2 −33:45:48	47658	60	
FCCB 1284	03:38:48.2 −32:42:09	39398	63		FCCB 1892	03:46:29.1 −34:24:21	16285	31	
FCCB 1299	03:38:52.9 −37:30:09	18980	23		FCCB 1898	03:46:30.6 −34:22:46	16130	73	
FCCB 1303	03:38:59.1 −36:15:03	34702	79		FCCB 1905	03:46:32.1 −36:53:41	18101	105	
FCCB 1306	03:39:03.7 −35:44:20	14838	47		FCCB 1903	03:46:34.6 −34:23:01	15664	61	
FCCB 1316	03:39:08.2 −35:52:17	25865	44		FCCB 1921	03:46:41.0 −36:56:43	18258	47	*
FCCB 1308	03:39:08.4 −33:30:16	15698	58	*	FCCB 1919	03:46:41.5 −35:51:35	23558	71	
FCCB 1315	03:39:11.6 −33:03:15	32347	97		FCCB 1911	03:46:43.8 −32:48:44	35132	68	
FCCB 1319	03:39:12.8 −34:07:09	16002	50		FCCB 1932	03:46:49.3 −36:26:45	21247	116	
FCCB 1321	03:39:14.8 −35:15:48	18459	64		FCCB 1939	03:46:56.0 −35:14:15	37814	153	
FCCB 1320	03:39:17.7 −32:51:27	28276	57		FCCB 1941	03:46:56.5 −35:46:17	25791	88	*
FCCB 1323	03:39:20.0 −34:27:38	21624	111		FCCB 1940	03:46:56.8 −35:15:03	37596	74	
FCCB 1335	03:39:22.8 −38:12:12	30910	53		FCCB 1942	03:46:58.2 −34:47:59	27823	88	
FCCB 1330	03:39:26.0 −34:19:18	37032	64	*	FCCB 1946	03:47:01.4 −34:26:27	15993	112	*
FCCB 1332	03:39:26.4 −34:51:52	26789	71		FCCB 1951	03:47:09.2 −32:49:22	27361	65	
FCCB 1339	03:39:31.6 −33:06:43	32728	83		FCCB 1974	03:47:18.5 −38:22:47	16325	134	
FCCB 1348	03:39:31.6 −36:53:18	14546	106		FCCB 1986	03:47:35.8 −37:29:31	23404	82	*
FCCB 1349	03:39:38.2 −32:37:08	38362	47		FCCB 1983	03:47:37.6 −34:16:55	19188	38	
FCCB 1353	03:39:39.0 −35:25:14	13850	37		FCCB 1984	03:47:38.0 −34:21:26	16381	134	
FCCB 1357	03:39:41.6 −33:52:37	16356	34		FCCB 1987	03:47:40.0 −35:25:03	35385	55	
FCCB 1355	03:39:43.4 −32:25:50	29330	58		FCCB 1988	03:47:42.6 −35:06:24	15255	30	
FCCB 1378	03:39:45.9 −37:50:41	25015	66		FCCB 1993	03:47:44.2 −36:08:47	23677	64	
FCCB 1373	03:39:46.0 −36:10:47	14693	64		FCCB 2007	03:47:50.8 −37:38:31	14153	69	
FCCB 1383	03:39:52.3 −36:59:43	42520	69		FCCB 2005	03:47:52.4 −36:06:60	23180	36	
FCCB 1377	03:39:52.4 −33:13:14	27581	33		FCCB 2020	03:48:06.1 −33:50:02	33124	77	
FCCB 1380	03:39:55.9 −32:24:49	63367	142		FCCB 2032	03:48:15.5 −34:30:14	15806	48	
FCCB 1384	03:39:56.5 −35:53:16	35941	42		FCCB 2037	03:48:16.4 −36:05:25	30270	118	
FCCB 1396	03:40:02.1 −37:47:31	13809	55		FCCB 2050	03:48:28.9 −33:19:44	35242	57	*

Table A2 – *continued*

FCC	RA (J2000) Dec	cz	σ_{cz}	cdE	FCC	RA (J2000) Dec	cz	σ_{cz}	cdE
FCCB 1389	03:40:03.8 −32:56:53	17794	55		FCCB 2047	03:48:29.2 −32:05:20	21665	62	
FCCB 1404	03:40:05.2 −37:47:32	13800	49		FCCB 2051	03:48:30.8 −32:14:21	21731	62	
FCCB 1399	03:40:05.6 −36:17:12	40193	45		FCCB 2058	03:48:34.9 −33:43:55	16005	12	
FCCB 1406	03:40:07.1 −37:08:59	24391	45	*	FCCB 2064	03:48:39.3 −34:02:48	49439	47	
FCCB 1407	03:40:09.1 −36:05:58	25652	70		FCCB 2063	03:48:39.5 −33:44:13	16193	27	
FCCB 1411	03:40:10.4 −37:49:40	14099	47	*	FCCB 2067	03:48:40.9 −35:54:45	18764	33	
FCCB 1408	03:40:13.6 −33:43:42	22104	48		FCCB 2087	03:48:56.5 −35:50:59	23125	104	
FCCB 1421	03:40:19.5 −37:14:17	14241	82		FCCB 2080	03:48:57.2 −32:37:17	22075	53	
FCCB 1419	03:40:24.7 −32:34:49	28579	47		FCCB 2092	03:49:02.2 −35:20:57	12181	31	
FCCB 1430	03:40:27.4 −37:49:56	12983	44		FCCB 2098	03:49:02.6 −36:26:08	34292	152	
FCCB 1436	03:40:30.4 −37:49:40	12855	39		FCCB 2096	03:49:03.5 −35:36:21	18103	46	
FCCB 1426	03:40:32.7 −33:05:13	21844	59	*	FCCB 2111	03:49:11.9 −36:33:40	5679	35	
FCCB 1446	03:40:42.8 −33:55:47	15986	39		FCCB 2138	03:49:43.7 −36:22:20	34835	63	
FCCB 1452	03:40:49.7 −35:33:24	14669	87		FCCB 2174	03:50:22.2 −33:56:53	7096	47	
FCCB 1454	03:40:53.1 −34:25:28	52838	41		FCCB 2180	03:50:29.4 −34:15:13	38068	135	
FCCB 1456	03:40:55.8 −33:10:01	42490	97		FCCB 2203	03:50:44.4 −37:22:32	23150	86	
FCCB 1467	03:41:03.8 −34:15:15	36937	74		FCCB 2197	03:50:45.1 −35:56:27	23107	32	
Name 5	03:41:11.5 −36:45:50	31302	36		FCCB 2199	03:50:49.2 −33:33:59	27597	127	
FCCB 1487	03:41:13.9 −37:45:05	34196	59		FCCB 2225	03:51:02.0 −36:01:39	18100	22	
FCCB 1498	03:41:21.1 −36:41:01	15170	28		FCCB 2230	03:51:11.9 −33:50:10	19380	77	
FCCB 1523	03:41:35.0 −36:16:50	6794	102		FCCB 2234	03:51:14.1 −34:25:27	16313	43	*
FCCB 1520	03:41:36.5 −33:40:58	21744	50		FCCB 2235	03:51:15.3 −33:49:02	19285	43	
FCCB 1528	03:41:36.5 −38:00:53	13664	45		Name 6	03:51:17.1 −35:45:49	18102	51	
FCCB 1538	03:41:42.2 −37:55:29	13681	38		FCCB 2239	03:51:21.0 −32:46:00	22340	47	*
FCCB 1532	03:41:43.0 −34:07:26	12161	62		FCCB 2248	03:51:22.3 −37:07:40	22473	42	
FCCB 1533	03:41:43.3 −34:29:41	37316	43		FCCB 2251	03:51:24.9 −37:20:22	16669	32	*
FCCB 1541	03:41:48.2 −36:48:51	8377	69	*	FCCB 2263	03:51:37.4 −34:54:11	18466	35	
FCCB 1548	03:41:57.2 −32:45:08	11534	64		FCCB 2276	03:51:50.1 −37:36:25	19162	39	
FCCB 1562	03:41:59.9 −38:01:57	13540	38		Name 7	03:51:59.5 −36:14:20	14505	34	
FCCB 1577	03:42:06.6 −36:38:20	15426	57		FCCB 2289	03:52:13.2 −33:25:09	22390	181	*
FCCB 1594	03:42:32.6 −33:12:17	19474	57		FCCB 2290	03:52:16.4 −32:07:22	10083	62	*

Notes: the names of the galaxies not listed in the FCC are given in Table 7. The asterisks indicate cdE candidates from the FCC.

selection criteria. We list these 408 background galaxies in Table A1.

We note that there are two background clusters identified behind the central region of the Fornax Cluster: a poor cluster at $z = 0.11$ (Hilker et al. 1999) and a more distant cluster ('J1556.15BL') at unknown redshift (Couch et al. 1991). Neither of these are evident in our data, the first because the members are fainter than our magnitude limit and the second, presumably, because it is at too high a redshift.

This paper has been typeset from a TEX/LATEX file prepared by the author.